

**Simulation of a
Turbo Charged Spark Ignited Engine
LiTH-ISY-EX-3010**

Examensarbete utfört i Fordonssystem
vid Tekniska Högskolan i Linköping
av

Fredrik Pettersson

Reg nr: LiTH-ISY-EX-3010

**Simulation of a
Turbo Charged Spark Ignited Engine
LiTH-ISY-EX-3010**

Examensarbete utfört i Fordonssystem
vid Tekniska Högskolan i Linköping
av


Fredrik Pettersson

Reg nr: LiTH-ISY-EX-3010

Supervisor: **Lars Eriksson**

Examiner: **Lars Eriksson**

Linköping, May 9, 2000.

	Avdelning, Institution Division, Department Vehicular Systems Dept. of Electrical Engineering	Datum: Date: 2000-05-05
	Språk Language <input type="checkbox"/> Svenska/Swedish <input checked="" type="checkbox"/> Engelska/English <input type="checkbox"/> _____	Rapporttyp Report category <input type="checkbox"/> Licentiatavhandling <input checked="" type="checkbox"/> Examensarbete <input type="checkbox"/> C-uppsats <input type="checkbox"/> D-uppsats <input type="checkbox"/> Övrig rapport <input type="checkbox"/> _____
URL för elektronisk version http://www.fs.isy.liu.se/		
Titel: Simulering av en bensindriven turbomotor Title: Simulation of a Turbo Charged Spark Ignited Engine Författare: Fredrik Pettersson Author:		
Sammanfattning Abstract <p>Datorsimulering har blivit ett allt viktigare hjälpmedel i utvecklingen av nya bilmotorer. En modell av motorn som simuleras i realtid kan användas för t ex modellbaserad reglerdesign och diagnos. Med hjälp av effektiv reglering och ett tillförlitligt diagnosystem kan både bränsleförbrukning och utsläpp minska.</p> <p>Mätningarna, som ligger till grund för simuleringsmodellen, är gjorda på en bensindriven 2,3-liters SAAB turbomotor. För modelleringen är motorn uppdelad i delsystem. Trycken i de olika delsystemen liksom turbinens vinkelhastighet är centrala storheter som modelleras dynamiskt. Utöver dessa är bl a massflöde och temperaturer modellerade med statistiska relationer. Modellerna för motorns delsystem är framtagna genom kombination av fysikalisk modellering och "black-box"-modellering.</p> <p>Ekvationerna för varje delsystem är implementerade som block i Simulink. Blocken är sedan sammankopplade till en fullständig simuleringsmodell. Simuleringsresultaten är jämförda med data från mätningar på SAAB-motorn. De dynamiska modellerna ger bra överensstämmelse med mätdata. Godtagbara resultat erhålls i de flesta fall även för de statistiska modellerna, men några av dem behöver utvecklas ytterligare om simuleringsmodellen ska kunna användas för prediktering.</p> <p>Några förslag på vidareutveckling av modellen och intressanta tillämpningar ges också.</p>		
Nyckelord Keywords modeling, turbine, compressor, pressure, MVEM		

Abstract

Computer simulation has become an important part of the development of new automotive engines. A model of the engine which can be simulated online may be used for model based control and diagnosis. An effective control system and reliable diagnosis can lower both fuel consumption and emissions.

Measurements made on a SAAB 2.3 litres turbo charged spark ignited engine are the base of the simulation model. To enable physical modeling, the engine is divided into subsystems. The pressures in the subsystems and the angular speed of the turbine shaft are central properties that are modeled dynamically. In addition to these models, static models of e.g. temperatures and mass flow are developed. A combination of physical modeling and black box modeling has been used to establish the models of the subsystems.

The equations of every subsystem are implemented as blocks in Simulink and the blocks are then connected to obtain a complete simulation model. The results from the simulations are compared with data from the measurements. The dynamic models agree well with measured data. The static models do also give acceptable results in most cases, but some of them have to be developed further to make the model useful for predictive purposes.

Some suggestions for further development and interesting applications of the model are also given.

Acknowledgments

I would like to thank everyone at Vehicular Systems for a nice and stimulating time, especially my examiner Lars Eriksson for his encouragement and valuable ideas.

Per Andersson, Johan Bergström and Jan Brugård are gratefully acknowledged for all help in the lab and many fruitful discussions about modeling and simulation of engines.

Finally I would like to thank Erik Frisk for solving many of my problems in \LaTeX .

Linköping, May 2000

Fredrik Pettersson

Contents

1	Introduction	1
1.1	Introduction to Turbo Charged Engines	2
2	Engine Modeling	5
2.1	Model Overview	5
2.2	Air Filter	6
2.2.1	Mass Flow Model	6
2.2.2	Dynamic Pressure-Model	8
2.3	Intercooler	9
2.3.1	Dynamic Pressure-Model	9
2.3.2	Mass Flow Model	10
2.3.3	Temperature Model	10
2.4	Throttle	11
2.5	Intake Manifold	13
2.5.1	Dynamic Pressure-Model	13
2.5.2	Mass Flow Model	13
2.6	Combustion	14
2.7	Exhaust Manifold	15
2.7.1	Dynamic Pressure-Model	15
2.7.2	Temperature Model	16
2.8	Exhaust System	17
2.8.1	Mass Flow Model	17
2.8.2	Dynamic Pressure-Model	19
2.9	Turbocharger	19

2.9.1	Turbine	20
2.9.2	Compressor	22
2.9.3	Waste Gate	29
2.10	Model Summary	29
3	Simulation of System Dynamics	35
3.1	Subsystem Dynamics	36
3.1.1	Filling Dynamics	36
3.2	Total Dynamics	37
4	System Validation	41
4.1	Stationary Validation	41
4.1.1	Description of the Experiments	42
4.1.2	Evaluation of Measurement and Simulation Data	42
4.2	Dynamic Validation	44
5	Summary	53
5.1	Accomplishments	53
5.2	Future Challenges	54
A	Engine Simulation	57
A.1	Solving Ordinary Differential Equations	57
A.1.1	Euler's Method	58
A.1.2	Runge-Kutta Methods	58
A.1.3	A General Algorithm	59
A.1.4	Stiff Differential Equations	59
A.1.5	Stability of Solutions	60
A.2	Literature	60
B	User's Guide	61

Nomenclature

Symbol	Quantity (explanation)	Unit
M	Engine torque	Nm
M_c	Compressor load torque	Nm
M_r	Turbo friction torque	Nm
M_t	Turbine driving torque	Nm
\dot{m}_{af}	Mass flow through air filter	kg/s
\dot{m}_{ac}	Air mass flow into the cylinders	kg/s
\dot{m}_c	Mass flow through compressor	kg/s
\dot{m}_{es}	Mass flow out of exhaust system	kg/s
\dot{m}_{fc}	Fuel mass flow into the cylinders	kg/s
\dot{m}_t	Mass flow through turbine	kg/s
\dot{m}_{th}	Mass flow through throttle	kg/s
\dot{m}_{wg}	Mass flow through waste gate	kg/s
N	Engine speed	RPM
P	Engine power	kW
p_{af}	Pressure after air filter	Pa
p_{amb}	Ambient pressure	Pa
p_c	Pressure after compressor outlet	Pa
p_{inter}	Pressure after intercooler	Pa
p_e	Pressure after exhaust valves	Pa
p_t	Pressure after turbine outlet	Pa
p_{th}	Pressure after throttle	Pa
T_{af}	Temperature after air filter	K
T_{amb}	Ambient temperature	K
T_c	Temperature after compressor outlet	K
T_{inter}	Temperature after intercooler	K
T_e	Temperature after exhaust valves	K
T_t	Temperature after turbine outlet	K
T_{th}	Temperature after throttle	K
V_{af}	Volume after air filter	m^3
V_c	Volume after compressor outlet	m^3
V_d	Displaced volume	m^3
V_{inter}	Volume after intercooler	m^3
V_e	Volume after exhaust valves	m^3
V_{es}	Volume of exhaust system	m^3
V_{th}	Volume after throttle	m^3
η_c	Compressor efficiency	-
η_{comb}	Combustion efficiency	-
η_t	Turbine efficiency	-
η_{vol}	Volumetric efficiency	-
ω_{tc}	Turbine shaft angular velocity	rad/s
θ_{tc}	Turbo moment of inertia	Nm^2

Chapter 1

Introduction

Simulation has, due to the increasing computational power of computers, become an important part of the development of new automotive engines. Engine simulations can be used to develop model based control systems, test new control strategies and for diagnosis. With increasing demands on low emissions and fuel consumption it will be necessary to predict the behavior of the engine and detect faults. One way to do this is to use an online simulation of the engine and compare the simulation results with values from measurements of the engine.

Given this background, it is interesting to develop a complete engine model which can be simulated by using a general simulation tool, in this case *Simulink*. The main goal of this project has been to develop a simulation model of a turbo charged spark ignited (SI) engine by combining models of the subsystems. In order to get good simulation results, it is extremely important to have good models of the different engine parts. The most crucial part to model is, from my experience, the turbocharger. In this thesis project physical modeling in combination with black box modeling have been used to develop the turbocharger model. A great deal of work has been done to accomplish a model that covers the whole operating region of the turbocharger.

Models for the turbocharger and the other engine components are calculated and presented in Chapter 2. Various aspects of simulation of dynamic systems are discussed in Appendix A. The simulation model is validated in Chapter 4 and finally, a brief summary is given in Chapter 5.

1.1 Introduction to Turbo Charged Engines

There are several text books about SI-engines. One book which discusses most aspects of internal combustion engines is [6], and it can indeed be recommended. A more concise description of SI-engines is given in [10] and it is a more easily accessible introduction to SI-engines than the book by Heywood. Good text books about turbo charged SI-engines are not as common as those about naturally aspirated SI-engines. One book which treats turbo charged internal combustion engines in general is [12] and it has been very useful in this project. The material in the following introduction to turbo charged engines can be found in both [6] and [12].

The power output from an internal combustion engine is proportional to the amount of air inducted into the cylinders. For a given engine speed, the amount of air inducted into the cylinders is proportional to the air density. In a conventional (naturally aspirated) engine, the pressure in the intake system is always smaller than or equal to the ambient pressure and the density of the intake air is hence lower than or equal to the density of the ambient air. One way to increase the density of the intake air is to boost the pressure in the intake system. This is usually done by a compressor. This concept of increasing the pressure in the intake system is called super charging. One way of super charging is to extract the power in the exhaust gases using a turbine. This method - consequently called turbo charging - is used on the SAAB engine, which is modeled in this project.

In the turbocharger the energy in the exhaust gases drives the turbine which in turn creates a driving torque on the turbine shaft. The turbine is connected to a compressor via the turbine shaft and hence the pumping capacity of the compressor depends on the amount of energy that the turbine can transmit from the exhaust gases. The turbine shaft speed is governed by the balance between the compressor power requirement and the turbine output power. There are also frictional losses in the turbocharger and accordingly some of the energy in the exhaust gases is dissipated while the rest is transmitted to the intake air. If the driving conditions of the engine are changed, the turbine shaft speed will change until a new equilibrium state has been reached.

Compression ignited (CI) engines, i.e. diesel engines, have been turbo charged for more than fifty years, while turbo charged spark ignited (SI) engines, i.e. gasoline engines, have become common in production cars only during the last two decades.

The main reason for this is probably that it is more difficult and less advantageous to turbo charge an SI-engine because of *knock*. In an SI-engine a homogeneous mixture of air and fuel is compressed in the cylinder. Normally a spark initiates the combustion which then spreads throughout the air-fuel mixture. Knocking occurs when the compression ratio, and consequently the temperature, has reached such a high level that the unburned end-gas self ignites before the flame front arrives. In this case, the combustion is very quick and causes severe pressure waves which may result in cylinder head and piston damage. To prevent knocking the temperature of the end-gas must be decreased which can be achieved by re-

ducing the compression ratio and sometimes also by adding an intercooler, which cools the inlet air.

Only air is compressed in the cylinder of a CI-engine. Fuel is sprayed directly into the combustion chamber only when combustion is required. The fuel is self-ignited and the compression ratio must therefore be high enough for the air temperature on compression to exceed the self-ignition temperature of the fuel. As the fuel injection takes time, there is only some of the fuel in the combustion chamber when the combustion starts and since much of the fuel has not fully vaporized or mixed with the air, the initial rate of combustion is not as damaging as the knocking situation in the SI-engine.

The gain in efficiency is most obvious in the case of turbo charging a CI-engine because the compression ratio does not need to be lowered, which is necessary in an SI-engine. For both engine types the pumping losses and friction decrease. The most important reason for turbo charging is though that the power to weight ratio increases and a turbo charged engine can hence be made smaller than a naturally aspirated engine for the same power output.

Chapter 2

Engine Modeling

2.1 Model Overview

When modeling a turbo charged SI-engine by using physical modeling, it is beneficial to divide the engine in distinct subsystems. Figure 2.1 shows the subsystems used in this study. The mass flow through the engine is central in the modeling and therefore the path of the flow will be described here. The air enters the engine via the *air filter*, where dust and other particles are removed. The air filter is described in detail in Section 2.2. The clean air then enters the *compressor* where both pressure and temperature increase. Models for the compressor are developed in Section 2.9.2. The air temperature must be lowered in order to avoid knock. This is done with a heat exchanger, called *intercooler*, and it is further described in Section 2.3. The mass flow into the cylinders and thereby also the output power of the engine is controlled by the *throttle*. The throttle opening depends on the accelerator pedal position and the mass flow through it is modeled in Section 2.4. After the throttle, the air enters the *intake manifold* where the fuel is injected. The properties of the intake manifold are discussed in Section 2.5. Then the air-fuel-mixture goes into the cylinders (denoted engine in the figure) where the *combustion* takes place. The combustion process is very complicated and a simple model of it is presented in Section 2.6. The hot exhaust gases then enter the *exhaust manifold* which is treated in Section 2.7. From the exhaust manifold the exhaust gases proceed either through the *turbine* or through the *waste gate*. These subsystems are modeled in Sections 2.9.1 and 2.9.3, respectively. The *exhaust system* (denoted catalyst in the figure) consists mainly of the catalyst and the silencer. Some interesting properties of the exhaust system are mentioned in Section 2.8.

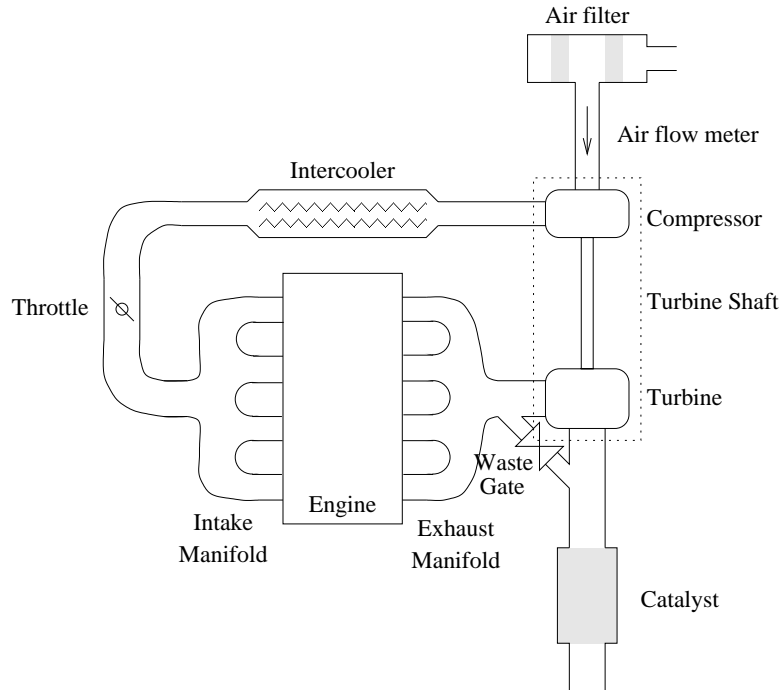


Figure 2.1 Sketch of a turbo charged SI-engine. The figure illustrates how the engine is divided into subsystems to enable physical modeling of the engine.

2.2 Air Filter

An air filter is used for one purpose; namely cleaning the intake air from pollutants. When the air is filtered, it has to pass through a flow restriction which causes a pressure loss. The modeling can be divided into a static part for the mass flow and a dynamic part for the pressure.

2.2.1 Mass Flow Model

The air filter can be modeled as a tube filled with a porous medium and therefore d'Arcy's law applies

$$p(t) = R_f Q(t) \quad (2.1)$$

where $Q(t)$ is the volumetric flow and R_f is called the flow resistance. D'Arcy's law does not hold if the flow is not laminar. If the tube contains a sudden change in area we have the approximate relationship

$$p(t) = H \cdot Q^2(t) \cdot \text{sgn}(Q(t)) \quad (2.2)$$

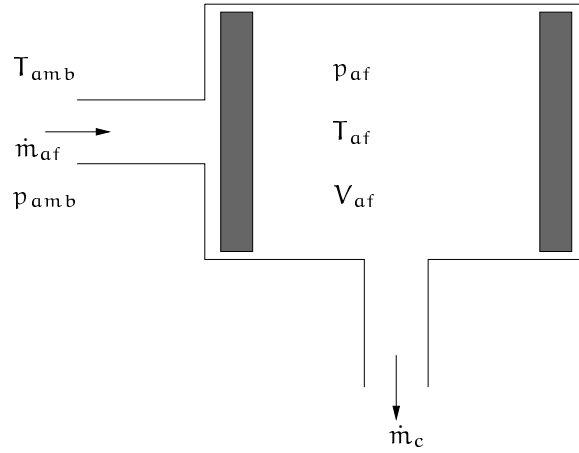


Figure 2.2 A sketch of the air filter. The grey areas represent the filter paper (flow restriction). The variables in the figure are necessary for the modeling of pressure loss and mass flow in the air filter.

for some constant H . The volumetric flow can be expressed as

$$Q = \frac{\dot{m}_{air}}{\rho}$$

For an ideal gas we have $\rho = \frac{p}{RT}$ and consequently

$$Q = \frac{\dot{m}_{air}RT}{p} \quad (2.3)$$

If Equation (2.3) is inserted into Equations (2.1) and (2.2) the total pressure loss over the air filter can be written as

$$p_{amb} - p_{af} = H_1 \cdot \left(\frac{\dot{m}_{air}RT_{amb}}{p_{amb}} \right) + H_2 \cdot \left(\frac{\dot{m}_{air}RT_{amb}}{p_{amb}} \right)^2 \quad (2.4)$$

for some constants H_1 and H_2 .

From correlation analysis the following model is also likely to give good agreement with measured data

$$p_{amb} - p_{af} = K T_{amb} \dot{m}_{af}^2 \quad (2.5)$$

Equations (2.4) and (2.5) have been tested [2] and especially Equation (2.4) gives good agreement with measured data, a validation is shown in Figure 2.3.

Inverting the static relationship Equation (2.4) yields the following expression for the mass flow through the air filter

$$\dot{m}_{af} = -\frac{\left(\frac{H_1 p_{amb}}{H_2 R T_{amb}} \right)}{2} + \sqrt{\left(\frac{\left(\frac{H_1 p_{amb}}{H_2 R T_{amb}} \right)}{2} \right)^2 + \frac{(p_{amb} - p_{af}) p_{amb}^2}{H_2 R^2 T_{amb}^2}} \quad (2.6)$$

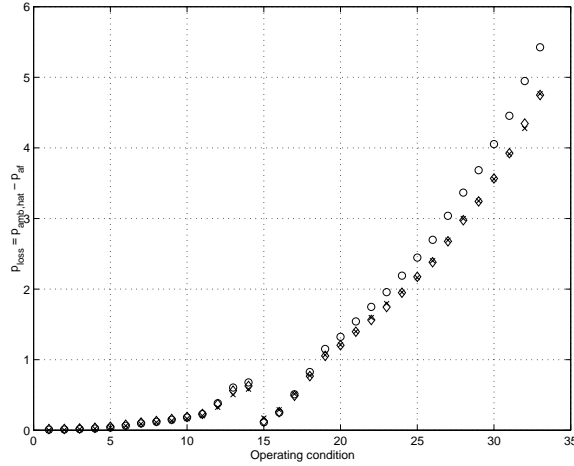


Figure 2.3 Validation plot for the pressure loss over the air filter. The validation points are denoted with x and Equation (2.4) is represented by \diamond . \circ represents Equation (2.5).

2.2.2 Dynamic Pressure-Model

The pressure at the end of the air filter varies significantly over time and must therefore be modeled. A straightforward way to model dynamics of this type is to use the method of emptying and filling tanks. The basic idea is to study mass conservation where the difference between the flow in to the tank and the flow out of the tank builds up or reduces the pressure. This can be calculated with *the ideal gas law*:

$$pV = mRT \quad (2.7)$$

The gas constant is assumed to be constant in the present temperature interval. Accordingly Equation (2.7) can be rewritten as

$$\Delta p = \frac{\Delta mRT}{V} \quad (2.8)$$

Differentiating Equation (2.8), inserting the variables from Figure 2.2, and also assuming $T_{af} = T_{amb}$, then we have

$$\frac{\partial p_{af}}{\partial t} = \frac{RT_{amb}}{V_{af}} (\dot{m}_{af} - \dot{m}_c) \quad (2.9)$$

The pressure can now be established through integration

$$p_{af} - p_{af,0} = \frac{RT_{amb}}{V_{af}} \int (\dot{m}_{af} - \dot{m}_c) dt$$

Where $p_{af,0}$ is the initial pressure after the air filter.

Equations (2.9) and (2.6) have been implemented in the simulation model.

2.3 Intercooler

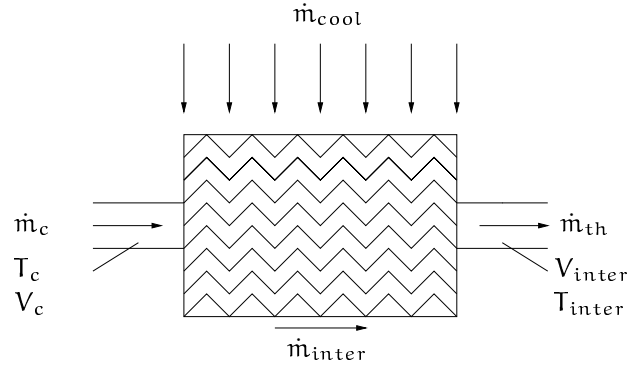


Figure 2.4 Sketch of the intercooler. The zigzag lines symbolize the thin cooling tubes of the intercooler and it is in these tubes the pressure loss in the intercooler arises.

The most important reason for turbo charging is to increase the power output of an engine without increasing its size. When the intake air is compressed, the density of the air increases and subsequently the mass of air-fuel-mixture drawn into the cylinders during the intake stroke rises. As a result, the output torque of the engine is boosted. However, it is not possible to compress air without raising its temperature, unless the compressor is cooled. This phenomenon is governed by *the first law of thermodynamics*¹ and reduces to some extent the benefits of turbo charging. The relation

$$\rho = \frac{P}{RT}$$

describes the phenomenon quantitatively.

If the temperature of the charge air is too high, the undesired phenomenon knock may occur in the combustion chamber. Knock is described in Section 1.1.

These two problems can obviously be dealt with if the charge air is cooled. This can be done with an intercooler which simply is a heat exchanger. In the case of automotive engines, the cooling medium is mostly air and thus the cooling effect gets larger at higher speeds when the air drag is greater.

The construction of a dynamic simulation model requires models for the pressure loss in the intercooler and the cooling effect of the intercooler.

2.3.1 Dynamic Pressure-Model

In the intercooler the air flows through a set of thin tubes. These tubes can be regarded as a static flow restriction. The dynamic properties of the intercooler are

¹For any cycle of a closed system, the net heat transfer equals the net work.

mainly due to the thicker tubes which connect the intercooler with the compressor and the intake system.

The pressure in the entering tube can be established in the same way as the pressure in the air filter was calculated in the previous section

$$\frac{\partial p_c}{\partial t} = \frac{RT_c}{V_c} (\dot{m}_c - \dot{m}_{inter}) \quad (2.10)$$

The pressure in the tube that leaves the intercooler can be calculated analogously

$$\frac{\partial p_{inter}}{\partial t} = \frac{RT_{inter}}{V_{inter}} (\dot{m}_{inter} - \dot{m}_{th}) \quad (2.11)$$

2.3.2 Mass Flow Model

[2] have evaluated several static relations for the pressure loss in the intercooler. They found that the following model works well

$$p_c - p_{inter} = kT_c \dot{m}_{inter}^2 \quad (2.12)$$

To make this model fit into the simulation model it has to be manipulated to

$$\dot{m}_{inter} = \sqrt{\frac{p_c - p_{inter}}{kT_c}} \quad (2.13)$$

Another tested model is

$$p_c - p_{inter} = k \left(\frac{T_c \dot{m}_{inter}}{p_c} \right)^2 \quad (2.14)$$

This model was however rejected as it does not give better fit to measured data than Equation (2.13) despite being, somewhat, more complicated.

In Figure 2.5 a validation plot of Equations (2.12) and (2.14) is shown.

The pressure model in the simulation model consists of Equations (2.10), (2.11) and (2.13).

2.3.3 Temperature Model

The ability of the intercooler to lower the temperature of the compressed air depends on the intercooler efficiency, ϵ , which is defined as

$$\epsilon = \frac{\text{actual heat transfer}}{\text{maximum possible heat transfer}}$$

For a perfect gas the heat capacity is a function of the temperature only and therefore the efficiency can be expressed, equivalently, as

$$\epsilon = \frac{T_c - T_{inter}}{T_c - T_{cool}}$$

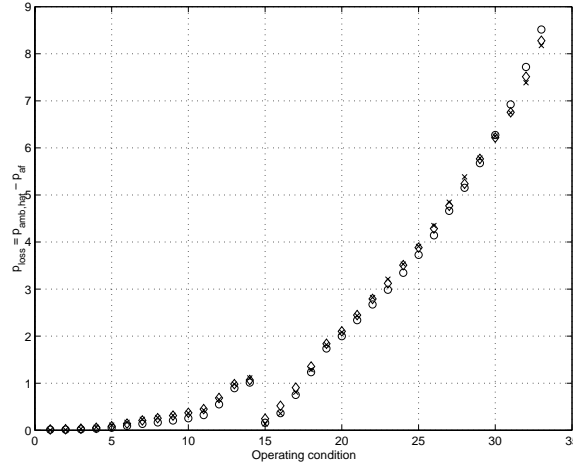


Figure 2.5 Validation plot of the pressure loss in the intercooler. The validation points are denoted with x and Equation (2.12) is represented by \diamond . \circ represents Equation (2.14).

This assumption is valid since c_p is equal for both the cooling medium and the air inside the intercooler - it is air in both cases. If $T_{inter} = T_{cool}$ the efficiency is, of course, one. The parameter of interest here is T_{inter} , and it can be put like

$$T_{inter} = T_c - \epsilon (T_c - T_{cool}) \quad (2.15)$$

An expression for ϵ can be found either by using solely physical modeling or by adjusting some grey box model to measured data. [2] tried both of these approaches. They found that the grey box model corresponds to measured data slightly better but, it might lack some of the generality of the purely physical model. Therefore the following grey box model has been chosen here.

$$\epsilon = k_0 + k_1 \left(\frac{T_c + T_{cool}}{2} \right) + k_2 \dot{m}_{inter} + k_3 \frac{\dot{m}_{inter}}{\dot{m}_{cool}} \quad (2.16)$$

Equation (2.15) is implemented together with Equation (2.16) in the simulation model.

2.4 Throttle

In gasoline engines a throttle is used to control the air mass flow into the cylinders. The mass flow through the throttle can be modeled like the flow of an ideal gas through a venturi. A standard model for this type of flow, see e.g. [10], is

$$\dot{m}_{th} = \frac{p_{inter}}{\sqrt{RT_{inter}}} A \cdot C \cdot \Psi(p_r) \quad (2.17)$$

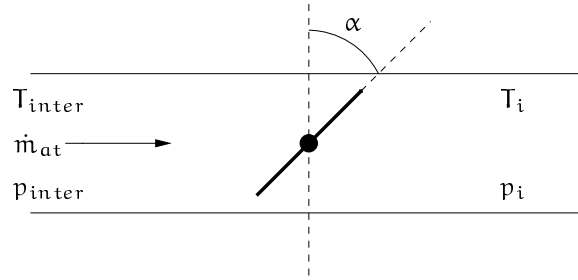


Figure 2.6 Sketch of the throttle. The throttle angle α governs the mass flow into the cylinders and hence the power output from the engine. The throttle angle, temperatures and pressures shown in the figure are used in a model for the mass flow through the throttle.

where A is the opening area, C is a discharge coefficient which depends on the shape of the flow area, and $\Psi(p_r)$ is a function of the pressure ratio

$$p_r = \frac{p_i}{p_{inter}}$$

The function Ψ looks like

$$\Psi(p_r) = \begin{cases} \sqrt{\frac{2\gamma}{\gamma-1} \left(p_r^{\frac{2}{\gamma}} - p_r^{\frac{\gamma+1}{\gamma}} \right)} & \text{if } p_r > \left(\frac{2}{\gamma+1} \right)^{\frac{\gamma}{\gamma-1}} \\ \sqrt{\frac{2\gamma}{\gamma-1} \left(\left(\frac{2}{\gamma+1} \right)^{\frac{2}{\gamma-1}} - \left(\frac{2}{\gamma+1} \right)^{\frac{\gamma+1}{\gamma-1}} \right)} & \text{otherwise} \end{cases} \quad (2.18)$$

where the pressure

$$p_{r,crit} = \left(\frac{2}{\gamma+1} \right)^{\frac{\gamma}{\gamma-1}}$$

is the critical pressure at which the air reaches sonic velocity in the restriction. For pressure ratios over $p_{r,crit}$, which is about 0.5, the second expression of Equation (2.18) is valid.

Both the opening area, A , and the discharge coefficient, C , depend to the greatest extent on the throttle plate opening angle α . A and C can for that reason be lumped together to a function $Q_{th}(\alpha)$. Hence Equation (2.17) transforms into

$$\dot{m}_{th}(\alpha, p_{inter}, p_i, T_{inter}) = \frac{p_{inter}}{\sqrt{RT_{inter}}} Q_{th}(\alpha) \Psi(p_r) \quad (2.19)$$

It is convenient to use this parameterization since only $Q_{th}(\alpha)$ has to be determined from tests in a test bed. There are nevertheless many ways to construct $Q_{th}(\alpha)$. One model, suggested by [11], is

$$Q_{th} = Q_1(1 - \cos(a_0\alpha + a_1)) + Q_0 \quad (2.20)$$

[2] tested Equation (2.20) with other models and came to the conclusion that it works well in comparison with these, sometimes more complicated, models. The validation plot in Figure 2.7 shows satisfactory agreement between the model and measured data.

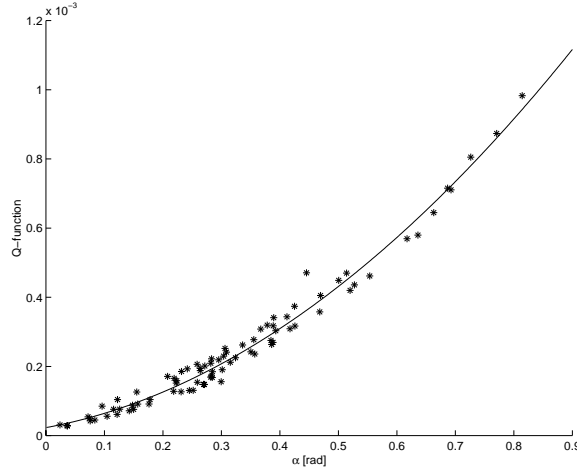


Figure 2.7 Validation plot for the Q -function. The solid line marks Equation (2.20) and * marks validation points. The figure shows that the throttle model works well.

Equation (2.19) has been implemented in the simulation model with $Q_{th}(\alpha)$ and $\Psi(p_r)$ in accordance with Equations (2.20) and (2.18), respectively.

2.5 Intake Manifold

2.5.1 Dynamic Pressure-Model

The dynamic properties of the intake manifold can be modeled with the same technique that was used for the dynamics of the intercooler. In this case the expression for the pressure becomes, $T_{inter} = T_{th}$,

$$\frac{\partial p_i}{\partial t} = \frac{RT_{inter}}{V_i} (\dot{m}_{th} - \dot{m}_{ac}) \quad (2.21)$$

2.5.2 Mass Flow Model

One of the parameters that governs the mass flow into the cylinders, \dot{m}_{ac} , is the volumetric efficiency, η_{vol} , which is a function of intake pressure, p_{th} , and engine speed, N . A plot of η_{vol} is given in Figure 2.8. As η_{vol} essentially is a function

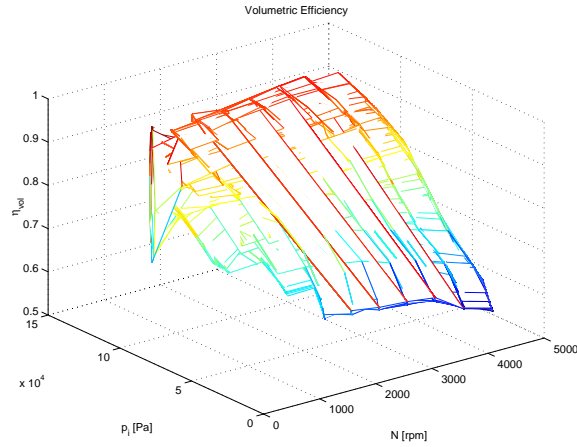


Figure 2.8 Volumetric Efficiency

of two variables, p_{th} and N , it is suitable to implement it as a two dimensional look-up table.

The other parameters that influence \dot{m}_{ac} are the displaced volume, V_d , and the temperature in the intake manifold, T_{th} . In a four stroke engine \dot{m}_{ac} can be calculated as

$$\dot{m}_{ac} = \frac{\eta_{vol}(N, p_{th}) V_d N p_{th}}{120RT_{th}} \quad (2.22)$$

where N is in [RPM]. Equation (2.22) is a standard model of \dot{m}_{ac} and it is discussed in more detail in e.g. [10].

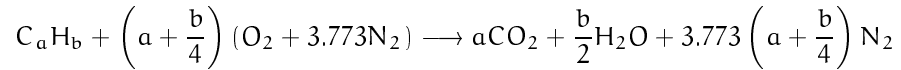
Equations (2.21), (2.22) and the look-up table for η_{vol} have been implemented in the simulation model.

2.6 Combustion

In order to inject a correct amount of fuel into the engine, it is necessary to know the theoretical proportions of air and fuel, i.e. there must be enough air to oxidize the fuel perfectly. This ratio is called the stoichiometric air to fuel ratio

$$\left(\frac{A}{F}\right)_s = \frac{m_{ac}}{m_{fc}}$$

The overall complete combustion reaction between a general hydro carbon $C_a H_b$ and air is



This combustion reaction defines the stoichiometric proportions of air and fuel. By denoting the relative contents of hydrogen and carbon in the fuel $y = \frac{b}{a}$ and using the molecular weights for carbon, hydrogen, oxygen and nitrogen we can derive the expression

$$\left(\frac{A}{F}\right)_s = \frac{(1 + y/4)(32 + 3.773 \cdot 28.16)}{12.011 + 1.008y} = \frac{34.56(4 + y)}{12.011 + 1.008y}$$

The petrol used in the laboratory has $(A/F)_s \approx 15$.

An interesting property is the ratio between the true air to fuel ratio, (A/F) , and $(A/F)_s$

$$\lambda = \frac{(A/F)}{(A/F)_s}$$

It is essential to keep λ close to one in order to maintain good catalyst function. It is only possible to have $\lambda = 1$ if $(A/F) = (A/F)_s$ and as a consequence we must have the following relation between the mass flow of air into the cylinders, \dot{m}_{ac} , and the mass flow of fuel into the cylinders, \dot{m}_{fc}

$$\dot{m}_{fc} = \frac{1}{15} \dot{m}_{ac} \quad (2.23)$$

When there is excess air in the combustion ($\lambda > 1$), the mixture is referred to as *lean* and when there is excess fuel in the combustion ($\lambda < 1$), the mixture is called *rich*. An engine that runs under lean conditions will emit large amounts of NO_x and if the mixture is rich there will inevitably be unburned hydro carbons and CO in the exhaust gases.

The engine torque, M , is a function of \dot{m}_{fc} , the heating value of the fuel, Q_{hv} , combustion efficiency, η_{comb} , and the engine speed, N . Hence the expression of M is defined as

$$M = \frac{\dot{m}_{fc} Q_{hv} \eta_{comb}}{2\pi N} \quad (2.24)$$

η_{comb} in its turn is a function of intake pressure, p_{th} , and N . Figure 2.9 shows how η_{comb} varies for different p_{th} and N .

A two dimensional look-up table has been utilized for the implementation of η_{comb} in the simulation model. Together with Equations (2.23) and (2.24) it forms the torque model.

The engine power, P , is easily calculated by

$$P = 2\pi MN$$

This expression is also implemented in the simulation model.

2.7 Exhaust Manifold

2.7.1 Dynamic Pressure-Model

The dynamics of the exhaust manifold can be described by the familiar tank model approach. The pressure in the manifold, p_e , is built up by the inflow \dot{m}_e and the

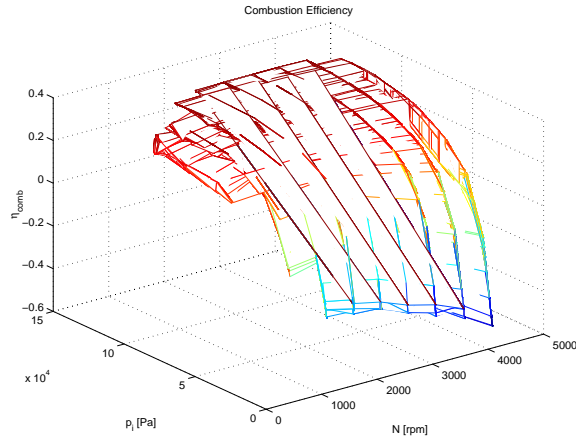


Figure 2.9 Combustion Efficiency

outflows \dot{m}_t and \dot{m}_{wg} . The temperature in the manifold is T_e and the volume is V_e . Thus we have

$$\frac{\partial p_e}{\partial t} = \frac{RT_e}{V_e} (\dot{m}_e - \dot{m}_t - \dot{m}_{wg}) \quad (2.25)$$

2.7.2 Temperature Model

The temperature in the exhaust manifold, T_e , can ideally be calculated in a straightforward way from the Otto cycle. However the Otto cycle does treat an adiabatic process but the process at hand here is, unfortunately not at all adiabatic. It is obvious that the heat transfer from the cylinders and the exhaust manifold to the surrounding air influences T_e greatly. As a consequence some other method, than the Otto cycle, must be found to describe the temperature changes in the manifold.

According to [6] the exhaust temperature increases with increasing engine speed, load, and spark retard, with speed being the variable with the largest impact. Different combinations of these properties have been tested as a model for T_e . Correlation analysis was used to find a combination of powers of N and M that works well. The following model seems to be a good trade off between high accuracy and low model order.

$$T_e = k_1 M^2 + k_2 \sqrt[4]{N} + k_3 MN \quad (2.26)$$

The temperature model, Equation (2.26), has been validated by using measured data and the result is plotted in Figure 2.10. In Figure 2.11 the difference between measured exhaust temperature and modeled exhaust temperature, i.e. the error, is plotted as a function of engine speed.

Equations (2.25) and (2.26) have been implemented in the simulation model.

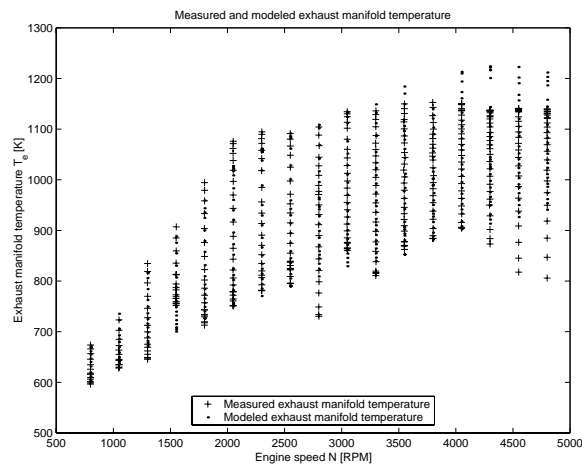


Figure 2.10 Measured exhaust manifold temperature and modeled exhaust temperature are plotted as functions of engine speed N .

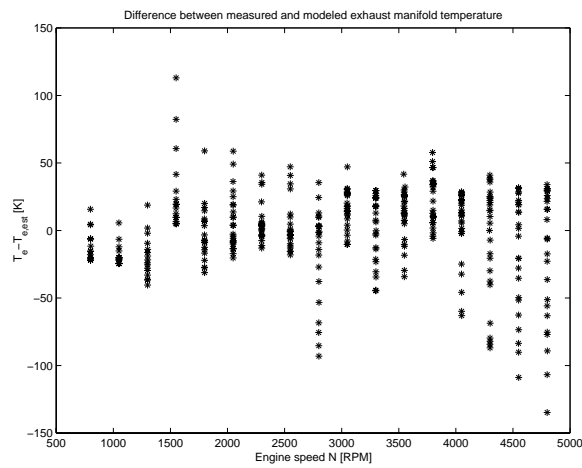


Figure 2.11 The figure shows the difference between measured exhaust temperature T_e and modeled exhaust temperature $T_{e,est}$ as a function of engine speed N .

2.8 Exhaust System

2.8.1 Mass Flow Model

There is a significant pressure drop from the turbine through the exhaust system to the surrounding air. As a consequence the pressure loss must be modeled. The

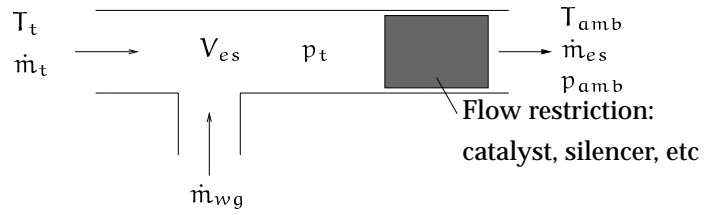


Figure 2.12 The exhaust gases enter the exhaust system from both the turbine and the waste gate. Due to the flow restriction in the exhaust system these flows build up a pressure, p_e , which needs to be modeled.

exhaust system can be seen as a tube with a sudden restriction, as illustrated in Figure 2.12. A suitable model for the flow through the restriction is

$$p_t - p_{amb} = k_1 \dot{m}_{es} T_t + k_2 \dot{m}_{es}^2 \quad (2.27)$$

The model has been validated by using measured data and the result is shown in Figure 2.13.

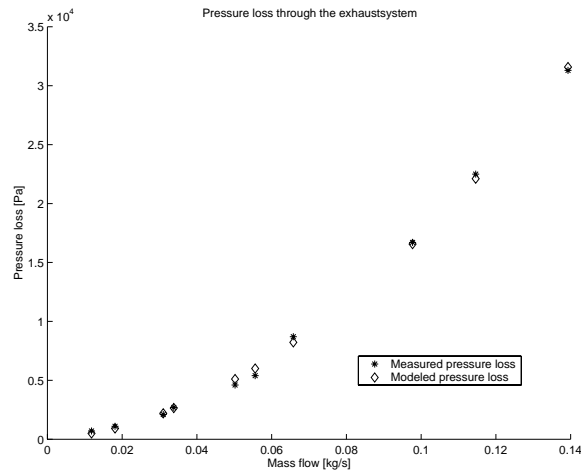


Figure 2.13 Validation plot for the exhaust system pressure model.

Equation (2.27) can be manipulated to

$$\dot{m}_{es} = -\frac{\left(\frac{k_1 T_t}{k_2}\right)}{2} + \sqrt{\left(\frac{\left(\frac{k_1 T_t}{k_2}\right)}{2}\right)^2 + \frac{p_t - p_{amb}}{k_2}} \quad (2.28)$$

2.8.2 Dynamic Pressure-Model

This expression works well together with the dynamic pressure model. The pressure is calculated as the integral of the mass flow differences in the same way as in the other pressure models presented in this report.

$$\frac{\partial p_t}{\partial t} = \frac{RT_t}{V_{es}} (\dot{m}_{wg} + \dot{m}_t - \dot{m}_{es}) \quad (2.29)$$

The exhaust system block in the simulation model consists of Equations (2.28) and (2.29).

2.9 Turbocharger

The exhaust gases from the engine create a driving torque $M_t(t)$ on the turbine shaft. The compressor load and frictional load from the bearings result in the torques $M_c(t)$ and $M_r(t)$, respectively. Newton's second law for rotating systems gives the following equation, where θ_{tc} is the moment of inertia of the turbocharger:

$$\dot{\omega}_{tc} = \frac{1}{\theta_{tc}} (M_t(t) - M_c(t) - M_r(t)) \quad (2.30)$$

The speed of the turbine shaft, ω_{tc} , can easily be obtained through integration from Equation (2.30). Equation (2.30) represents the dynamics of the turbine shaft.

The theoretical maximum torque delivered by the turbine depends on the temperature before the turbine, T_e , and the ratio between the pressure before the turbine, p_e , and the pressure after the turbine, p_t . If the process would be reversible, which means there would not be any frictional losses in the turbine, the work would be called isentropic. This is obviously not the case here, because the turbine gets red hot at high loads. A value of the level of the isentropic work that is actually used to propel the turbine shaft is the efficiency, η_t . The mass flow through the turbine is denoted \dot{m}_t . Considering the losses in the turbine [5] suggest the following model for the static properties of the turbine.

$$M_t \omega_{tc} = \eta_t \dot{m}_t c_p T_e \left[1 - \left(\frac{p_e}{p_t} \right)^{(1-\gamma)/\gamma} \right] \quad (2.31)$$

c_p stands for the specific heat capacity for constant pressure and γ denotes the ratio of specific heats c_p/c_v , where c_v is the specific heat capacity for constant volume. Since the turbine shaft speed, ω_{tc} , can be found through integration of Equation (2.30) it is possible to solve Equation (2.31) to yield M_t .

The load torque which results from the compressor can be calculated in a similar way as the driving torque on the turbine side of the turbocharger. Like the turbine, the compressor is not ideal and therefore we introduce the compressor efficiency, η_c . The load on the compressor depends on the pressure before the compressor, p_{af} , the pressure after the compressor, p_c , and the temperature before

the compressor, T_{af} . The following equation has been proposed by [5] as a model for the static properties of the compressor.

$$\eta_c M_c \omega_{tc} = \dot{m}_c c_p T_{af} \left[\left(\frac{p_c}{p_{af}} \right)^{(\gamma-1)/\gamma} - 1 \right] \quad (2.32)$$

Solving Equation (2.32) yields M_c .

Equation (2.32) together with Equation (2.31) model the static properties of the turbocharger.

Equations (2.30), (2.31) and (2.32) have been used by many authors, e.g. [5], and provide a physically reasonable and straightforward method to model the turbocharger and it is therefore chosen here. In the next two sections models for the mass flows, \dot{m} , efficiencies, η , and temperatures, T , for the turbine and compressor will be developed.

2.9.1 Turbine

Mass Flow Model

The mass flow through the turbine is practically turbine shaft speed independent and it turned out it could be accurately modeled by using only the pressure ratio, p_e/p_t , as regression parameter. When the pressure ratio is equal to one, there cannot be any mass flow through the turbine. Even a small mass flow requires a pressure difference between inlet and outlet which gives a physically interpretable limit. Modeling data provided by the manufacturer covers only pressure ratios over 1.15, but the limit of the mass flow requires extrapolation of the mass flow to zero at pressure ratio one. The shape of the mass flow and the boundary condition led to the following model structure

$$\dot{m}_t = k_1 \left(\frac{p_e}{p_t} - 1 \right) + k_2 \sqrt{\frac{p_e}{p_t} - 1} \quad (2.33)$$

Equation (2.33) is linear in parameters and the parameters can be adjusted to measured data by using standard least square methods. When one compares Equation (2.33) to other proposed model structures it seems to produce a reasonable trade off between low model order and ability to follow the varying mass flow. A low model order is desirable, as such a model is more likely to give acceptable extrapolation results compared to a higher order model. In Figure 2.14 it is obvious that Equation (2.33) matches the measured data very well and it has been implemented in the simulation model with good result.

Efficiency Model

The turbine efficiency data from the manufacturer is, as the mass flow plot, restricted to pressure ratios over 1.15. In the mass flow case it was straightforward to extrapolate to pressure ratio one because we knew a physical limit. This is not

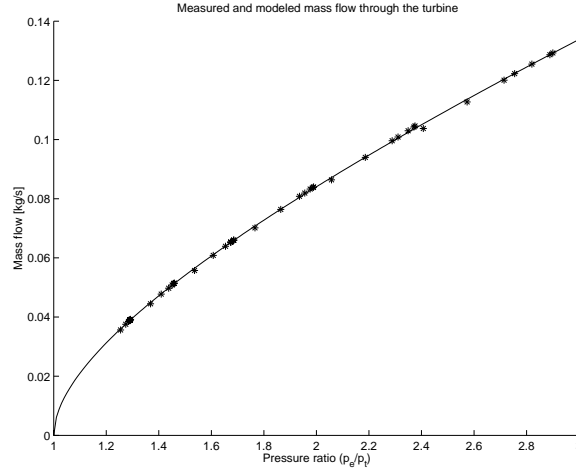


Figure 2.14 Validation plot for the turbine mass flow model. The solid line denotes modeled values of \dot{m}_t and * stands for measured data. There is clearly good agreement between the measurements and the model (Equation (2.33)).

the case for the efficiency. The question is: What is the efficiency when there is no mass flow through the turbine? It is hard to answer this question, but it seems likely that the efficiency decreases further when the pressure ratio approaches one. The influence of turbine shaft speed on the turbine efficiency is complicated and it is very difficult to develop a model which follows the measured efficiency in Figure 2.15 particularly well. For this reason, it is interesting to know if the efficiency follows the speed lines down to the lowest values for the efficiency or if the turbine shaft instead loses speed when the efficiency gets too low. This would lead to a shift of speed lines and thus increasing efficiency, see Figure 2.15. This is a topic that certainly has to be looked into in more detail. With the rough assumption that the efficiency is independent of the turbine shaft speed, several model structures are plausible, one is

$$\eta_t = k_1 \sqrt{\frac{p_e}{p_t} - 1} + k_2 \sqrt[4]{\frac{p_e}{p_t} - 1} + k_3 \quad (2.34)$$

In order to get a representative efficiency model, the point with lowest efficiency on every speed line was removed before the least square method was used. In the validation plot however, Figure 2.15, all measured data points are included. Clearly the model does not follow the efficiency variations in detail, but the model captures the overall behavior.

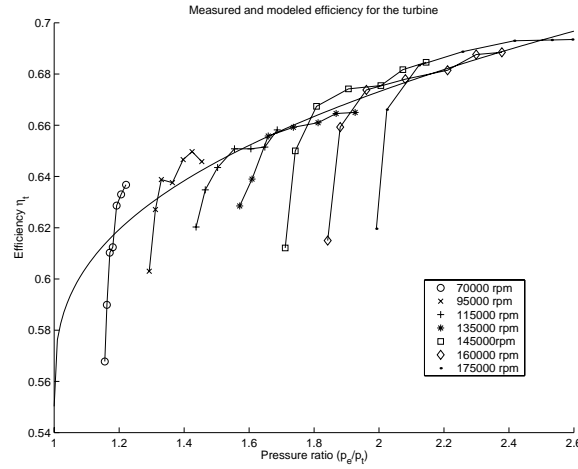


Figure 2.15 Validation plot for the turbine efficiency model.

Temperature Model

If the expansion of gases through the turbine was isentropic, i.e. $\eta_t = 1$, the temperature after the compressor could, according to [6], be modeled as

$$T_t = T_e \left(\frac{p_t}{p_e} \right)^{(\gamma-1)/\gamma} \quad (2.35)$$

The heat capacity, c_p , is assumed to be constant in this expression. Measurements on the engine show, as expected, that this ideal model does not hold. The great heat transfer from the turbine to the surroundings is the reason why Equation (2.35) fails to capture the behavior of T_t . A number of combinations of the ideal expression, Equation (2.35), and correction terms were tested. One model that turned out to work well was

$$T_t = k_1(T_e - T_{amb}) \left(\frac{p_t}{p_e} \right)^{(\gamma-1)/\gamma} + k_2(T_e - T_{amb})^2 + k_3 \quad (2.36)$$

In Figure 2.16 the modeled turbine temperature is compared to data from measurements. The model gives good agreement to the measurements over the whole operating region of the engine.

2.9.2 Compressor

Mass Flow Model

The compressor mass flow, pressure ratio and turbine shaft speed varies a lot between different loads. During normal driving the engine often works at low loads,

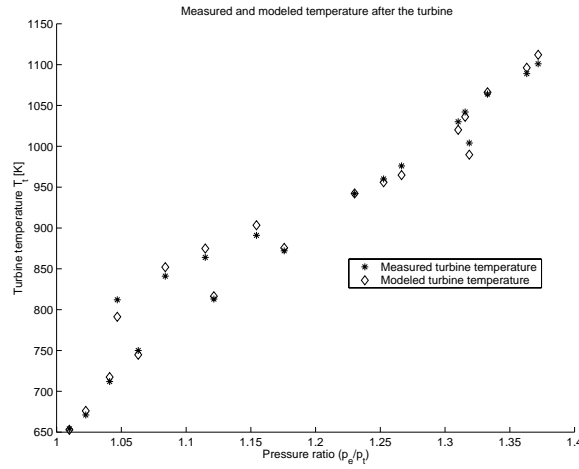


Figure 2.16 Validation plot for the turbine temperature model.

which means low pressure ratios and low turbine shaft speeds. For some reason this region of operation is not included in the compressor map provided by the manufacturer. The pressure ratio and turbine shaft speed interact in a complicated way to produce the mass flow and hence the mass flow is not easy to model using a polynomial. A few fruitful observations can however be made: \dot{m}_c is almost linearly dependent on ω_{tc} and increases with $\frac{p_{af}}{p_c}$. The mass flow through the compressor must be zero at times where no pressure difference between the compressor inlet and outlet is shown. This observation introduces a physical limit on the model. Correlation analysis was made to see which combinations of $\frac{p_{af}}{p_c}$ and ω_{tc} that have the greatest influence on \dot{m}_c . Finally, the following model structure was chosen.

$$\dot{m}_c = k_1 \left(1 - \frac{p_{af}}{p_c} \right) + k_2 \omega_{tc} \sqrt{1 - \frac{p_{af}}{p_c}} + k_3 \omega_{tc}^4 \sqrt{1 - \frac{p_{af}}{p_c}} + k_4 \omega_{tc} \quad (2.37)$$

The model is constructed from data provided by the turbocharger manufacturer and the data does not cover turbine shaft speeds under 80000 RPM. Therefore the model works best for medium to high turbine shaft speeds. The extrapolation capabilities down to turbine shaft speeds under 30000 RPM turn out to be quite bad, which can be seen in Section 4.1. In the region where the model is defined it does, however, work unexpectedly well, which can be seen in Figure 2.17. Equation (2.37) has been implemented in the simulation model.

Another way to get an acceptable model of \dot{m}_c is to use a two dimensional look-up table. If \dot{m}_c is mapped for $\frac{p_{af}}{p_c}$ and ω_{tc} over the whole operating region of the engine, the values for the efficiency within and outside the map can be found through interpolation and extrapolation, respectively. The interpolation and extrapolation are dealt with automatically in e.g. Simulink. Because of its simplicity,

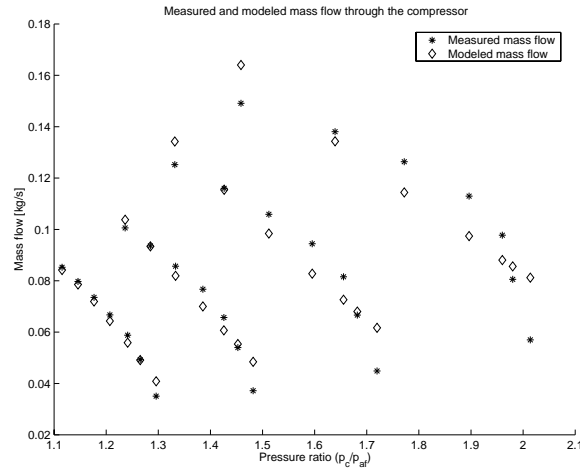


Figure 2.17 Validation plot of the compressor mass flow model. The groups of points represent turbine shaft speeds 80000 RPM, 100000 RPM, 120000 RPM and 140000 RPM, respectively. It is obvious that the model works best at the lowest turbine shaft speed lines in the figure.

look-up tables are often used in the industry. The reason why a look-up table is not used here is its shortage of physical background, which might result in worse extrapolation properties compared to a grey box model like Equation (2.37).

Efficiency Model

The compressor's only task is to compress air. Its efficiency can thereby be defined in terms of power requirement for doing this work

$$\eta_c = \frac{\text{reversible (isentropic) power requirement}}{\text{actual power requirement}}$$

Enthalpy h is a property with dimension energy and in this case it is suitable to use the ratio of differences in enthalpies as a measure of the efficiency.

With notations according to Figure 2.18 we have

$$\eta_{c,TT} = \frac{h_{02s} - h_{01}}{h_{02} - h_{01}}$$

The subscript TT denotes that this is an expression for the total-to-total isentropic efficiency, where total refers to the pressure. However, it is more accurate to use an expression for the total-to-static isentropic efficiency $\eta_{c,TS}$. The volume after the compressor is big which gives small flow velocities and thus the dynamic pressure becomes small.

$$\eta_{c,TS} = \frac{h_{2s} - h_{01}}{h_{02} - h_{01}}$$

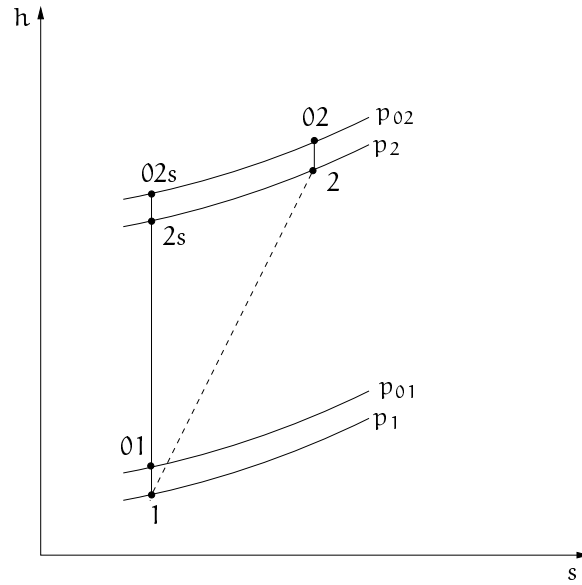


Figure 2.18 The figure shows the change in enthalpy as a function of the change in entropy (h - s -plot). p_{01} and p_1 represent initial total pressure and initial static pressure, respectively. p_{02} and p_2 stand for final total pressure and final static pressure, respectively. The vertical line illustrates the behavior of an ideal compressor (constant entropy) and the sloping line symbolizes the real case (increasing entropy).

By using this enthalpy-approach, the following model can be derived [2].

$$\eta_{c,TS} = \frac{U_c^2 \left(s_1 \left(\frac{\dot{m}_{air}}{U_c} \right)^2 + s_2 \left(\frac{\dot{m}_{air}}{U_c} \right) + s_3 \right)}{b_1 \dot{m}_{air} + b_2 \dot{m}_{air} U_c + b_3 U_c^2 + b_4 U_c + b_5} \quad (2.38)$$

U_c denotes the tip speed of the compressor. The numerator has been found through correlation analysis together with some physical insight. The denominator is a model that has frequently been used in other reports and may therefore be regarded as a standard model. Equation (2.38) is not particularly elegant with its eight parameters, but without any other model at hand, it is good enough. Anyway, Equation (2.38) corresponds well to measured data, as illustrated by Figure 2.19, and it has been implemented in the simulation model.

Temperature Model

The temperature rise through the compressor can be calculated using the same formula as for the turbine. The compressor temperature appears to follow the isentropic model even better than the turbine temperature. A probable explanation is

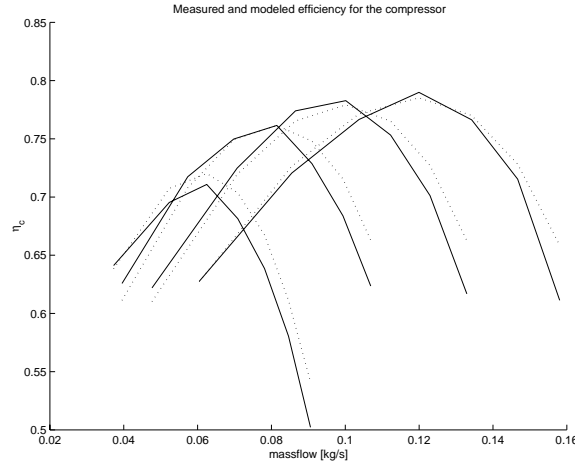


Figure 2.19 Validation plot of the compressor efficiency model. The dotted lines represent modeled values and the solid lines stand for measured data.

the compressor's higher efficiency in general which makes the isentropic approximation more appropriate in this case. Consequently a physically tractable model is

$$T_c = k_1 T_{af} \left(\frac{p_c}{p_{af}} \right)^{(\gamma-1)/\gamma} \quad (2.39)$$

Despite its simplicity, Equation (2.39) works well which can be seen in Figure 2.20. One problem with Equation (2.39) is its slight temperature rise at pressure ratio one as $k_1 \approx 1.05$.

Surge

A wide range of operation is of great importance when turbochargers are used in automobiles. The engine runs mostly at quite low loads during normal driving where the mass flow into the cylinders is low and consequently the boost pressure from the compressor is not particularly high. Turbochargers are designed to work first of all well at high engine loads and it is in this field the current turbocharger models work best. As the compressor is more sensitive for variations in mass flow and pressure ratios than the turbine, most stability problems of the turbocharger are due to the compressor. Figure 2.21 shows the operating area of the compressor. The stable operating zone lies between the unstable surge region on the left and the choking region on the right.

According to Figure 2.21 surge occurs when the mass flow is low and the pressure ratio between compressed air and the air from the air filter is high. The higher the pressure ratio is, the higher must the mass flow be to avoid surge. A thorough

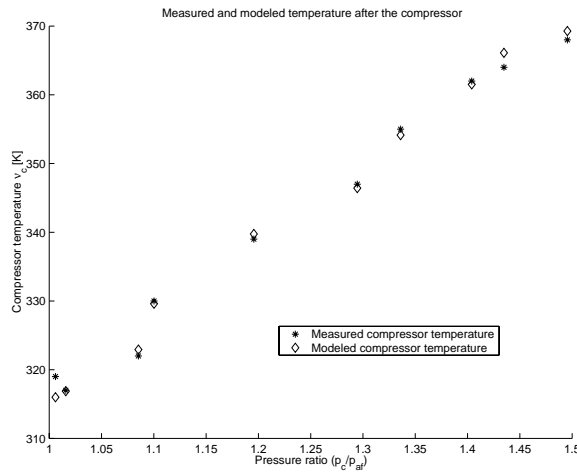


Figure 2.20 Validation plot of the compressor temperature model.

explanation of surge is given in [12] and the main guidelines are recapitulated here. Some interesting aspects of surge are mentioned in [9]. To study the flow through the compressor in detail gives a great deal of information about the physical properties, e.g. flow separation (stall), that cause surge. This approach requires a great deal of fluid mechanics to be done properly and will not be treated here.

Fortunately, the larger scale characteristics of surge can be understood by looking at the system of air filter, compressor and intake system. The constant speed lines in Figure 2.21 have negative derivative in the stable operating zone (except a part of the speed line of the highest turbine shaft speed in the figure). Imagine that the engine is running with wide open throttle, when a sudden partial closure of the throttle occurs. This results in increasing compressor pressure and decreasing mass flow, which move the operating point to the left. The rise in compressor pressure however forces more air through the throttle and increases the mass flow again, which in turn reduces the compressor pressure. The working point is now moved back towards the original point. This is therefore a self-compensating and inherently stable system.

The behavior is totally different in the unstable region to the left of the surge line. The constant speed lines exist in this region as well, but they have positive derivative here. The same throttle angle experiment can be carried out here just as in the stable operating zone. In this case a reduction in mass flow would result in reduced compressor pressure and thereby move the operating point further and further to the left. Eventually the energy imparted to the gas falls below the amount needed to overcome the adverse pressure gradient between inlet and outlet. The flow suddenly collapses, causing the output pressure to drop to a level at which it can be re-established. The mass flow will increase until the system is

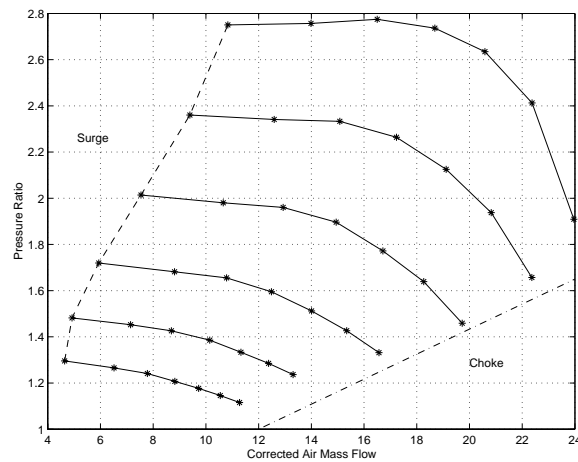


Figure 2.21 The figure illustrates the operating area of the compressor. The stable part is limited by the surge region to the left and by the choking region to the right. Note that the turbine shaft speed lines have negative derivative in the stable part. The turbine shaft speed lines continue into the surge part where they have positive derivative.

drawn back to the original operating point. Then the whole cycle will repeat itself.

The turbocharger manufacturers usually make their compressor performance plots from measurements done when the turbocharger is not connected to an engine. This is of course an idealized situation because the fluctuations in mass flow, due to periodic suction strokes from the pistons, are not considered. The intake system is sometimes too small to fully damp out these flow irregularities. Even though the mean mass flow rate lies to the right of a surge line obtained under steady flow compressor calibration tests, the minimum mass flow rate may cause surge to develop. Thus, when the turbocharger is connected to an engine, the fluctuations in mass flow can cause the surge line to shift to the right i.e. towards larger mass flows.

Choking

The stable operating zone is limited on the right by choking. When the mass flow increases, the velocity of the flow naturally increases as well. Eventually the flow will become sonic and no higher speed of the mass flow can be reached in the compressor. Extra mass flow through the compressor can be obtained only by higher turbine shaft speed. When the diffuser is choked, turbine shaft speed may rise substantially with only a limited increase in the mass flow rate [6].

2.9.3 Waste Gate

The turbocharger can easily overspeed at high loads, resulting in excessive boost pressure and even turbocharger bearing failure. If the pressure in the intake system gets too high knock will appear in the combustion chamber, as mentioned in Section 1.1. To prevent over speeding and knock, it is common to let some of the exhaust gases pass by the turbine directly into the exhaust system using a *waste gate*. The driving torque on the turbine and thus the turbine shaft speed will stay at a lower level when the waste gate is opened.

The waste gate is basically a valve, which is opened when the boost pressure from the compressor reaches a certain reference value. A simple model of the waste gate can be determined by using the same modeling approach as for the throttle in Section 2.4. The Ψ -function gives the mass flow as a function of the pressure ratio. If Ψ is multiplied with the controller amplification we will have a value of the mass flow through the waste gate. The controller amplification can be seen as a measure of the waste gate opening area.

In this thesis project a PI-controller is implemented to govern the waste gate opening area. The engine model is a non linear dynamic system. The PI-controller was initially tuned by using Ziegler-Nichols rules. This method for controller synthesis is described in further details in e.g. [4]. The Ziegler-Nichols rules did not give a controller with sufficiently good performance, but they gave a hint about the magnitudes of the controller parameters. The controller was for that reason tuned to give reasonable step response and no stationary control error. Tests at different speeds and loads have shown that the PI-controller works well and there is therefore no need to add a derivative part to the controller.

The waste gate behavior on a real engine is much more complicated than the simple controller implemented in the model. At low gears the torque on the drive shafts can reach damaging high levels and therefore a lower boost pressure reference value is often used to limit the torque. With more detailed information about the real controller it would, of course, be possible to create a more accurate model. There is also a pneumatic control system for the waste gate, which makes it even harder to know the exact control actions. Despite lack of knowledge when it comes to the pneumatic control system, the best solution is probably still to use program code from the current engine control system.

2.10 Model Summary

The model is summarized in this section to make it easier to get a complete picture of the model equations. There is a Matlab m-file where the values of all model parameters can be found. Therefore those values are not recapitulated here as they do not bring much information to the reader, but rather make the model summary look uglier.

In Figure 2.22 the path of the air through the engine is shown. The flow restrictions which are used to model the different pressures in the engine are displayed

in the sketch. In addition to the state variables (i.e. pressures and ω_{tc}), some other quantities which are central in the modeling are included in the figure.

The presentation order of the model equations follows the path of the air through the engine. Since the turbocharger is connected both to the inlet and the outlet of the engine it is presented at the end.

- Air Filter

$$\frac{\partial p_{af}}{\partial t} = \frac{RT_{amb}}{V_{af}} (\dot{m}_{af} - \dot{m}_c)$$

where \dot{m}_{af} is defined as

$$\dot{m}_{af} = -\frac{\left(\frac{H_1 p_{amb}}{H_2 R T_{amb}}\right)}{2} + \sqrt{\left(\frac{\left(\frac{H_1 p_{amb}}{H_2 R T_{amb}}\right)}{2}\right)^2 + \frac{(p_{amb} - p_{af})p_{amb}^2}{H_2 R^2 T_{amb}^2}}$$

- Intercooler

$$\frac{\partial p_c}{\partial t} = \frac{RT_c}{V_c} (\dot{m}_c - \dot{m}_{inter})$$

$$\frac{\partial p_{inter}}{\partial t} = \frac{RT_{inter}}{V_{inter}} (\dot{m}_{inter} - \dot{m}_{th})$$

In both expressions \dot{m}_{inter} has the form

$$\dot{m}_{inter} = \sqrt{\frac{p_c - p_{inter}}{kT_c}}$$

$$T_{inter} = T_c - \epsilon (T_c - T_{cool})$$

where ϵ is defined as

$$\epsilon = k_0 + k_1 \left(\frac{T_c + T_{cool}}{2}\right) + k_2 \dot{m}_{inter} + k_3 \frac{\dot{m}_{inter}}{\dot{m}_{cool}}$$

- Throttle

$$\dot{m}_{th}(\alpha, p_{inter}, p_i, T_{inter}) = \frac{p_{inter}}{\sqrt{RT_{inter}}} Q_{th}(\alpha) \Psi(p_r)$$

where $\Psi(p_r)$ looks like

$$\Psi(p_r) = \begin{cases} \sqrt{\frac{2\gamma}{\gamma-1} \left(p_r^{\frac{2}{\gamma}} - p_r^{\frac{\gamma+1}{\gamma}}\right)} & \text{if } p_r > \left(\frac{2}{\gamma+1}\right)^{\frac{2}{\gamma-1}} \\ \sqrt{\frac{2\gamma}{\gamma-1} \left(\left(\frac{2}{\gamma+1}\right)^{\frac{2}{\gamma-1}} - \left(\frac{2}{\gamma+1}\right)^{\frac{\gamma+1}{\gamma}}\right)} & \text{otherwise} \end{cases}$$

and Q_{th} has the form

$$Q_{th} = Q_1 (1 - \cos(a_0 \alpha + a_1)) + Q_0$$

- Intake Manifold

$$\frac{\partial p_i}{\partial t} = \frac{RT_{inter}}{V_i} (\dot{m}_{th} - \dot{m}_{ac})$$

where \dot{m}_{ac} looks like

$$\dot{m}_{ac} = \frac{\eta_{vol}(N, p_{th})V_d N p_{th}}{120RT_{th}}$$

- Combustion

$$M = \frac{\dot{m}_{fc} Q_{hv} \eta_{comb}}{2\pi N}$$

where \dot{m}_{fc} has the form

$$\dot{m}_{fc} = \frac{1}{15} \dot{m}_{ac}$$

$$P = 2\pi MN$$

- Exhaust manifold

$$\frac{\partial p_e}{\partial t} = \frac{RT_e}{V_e} (\dot{m}_e - \dot{m}_t - \dot{m}_{wg})$$

$$T_e = k_1 M^2 + k_2 \sqrt{N} + k_3 MN$$

- Exhaust System

$$\frac{\partial p_t}{\partial t} = \frac{RT_t}{V_{es}} (\dot{m}_{wg} + \dot{m}_t - \dot{m}_{es})$$

where \dot{m}_{es} looks like

$$\dot{m}_{es} = -\frac{\left(\frac{k_1 T_t}{k_2}\right)}{2} + \sqrt{\left(\frac{\left(\frac{k_1 T_t}{k_2}\right)}{2}\right)^2 + \frac{p_t - p_{amb}}{k_2}}$$

- Turbocharger

$$\dot{\omega}_{tc} = \frac{1}{\theta_{tc}} (M_t(t) - M_c(t) - M_r(t))$$

$$M_t \omega_{tc} = \eta_t \dot{m}_t c_p T_e \left[1 - \left(\frac{p_e}{p_t} \right)^{(1-\gamma)/\gamma} \right]$$

$$\eta_c M_c \omega_{tc} = \dot{m}_c c_p T_{af} \left[\left(\frac{p_c}{p_{af}} \right)^{(\gamma-1)/\gamma} - 1 \right]$$

- Turbine

$$\dot{m}_t = k_1 \left(\frac{p_e}{p_t} - 1 \right) + k_2 \sqrt{\frac{p_e}{p_t} - 1}$$

$$\eta_t = k_1 \sqrt{\frac{p_e}{p_t} - 1} + k_2 \sqrt[4]{\frac{p_e}{p_t} - 1} + k_3$$

$$T_t = k_1 (T_e - T_{amb}) \left(\frac{p_t}{p_e} \right)^{(\gamma-1)/\gamma} + k_2 (T_e - T_{amb})^2 + k_3$$

- Compressor

$$\dot{m}_c = k_1 \left(1 - \frac{p_{af}}{p_c} \right) + k_2 \omega_{tc} \sqrt{1 - \frac{p_{af}}{p_c}} + k_3 \omega_{tc} \sqrt[4]{1 - \frac{p_{af}}{p_c}} + k_4 \omega_{tc}$$

$$\eta_{c,TS} = \frac{U_c^2 \left(s_1 \left(\frac{\dot{m}_{air}}{U_c} \right)^2 + s_2 \left(\frac{\dot{m}_{air}}{U_c} \right) + s_3 \right)}{b_1 \dot{m}_{air} + b_2 \dot{m}_{air} U_c + b_3 U_c^2 + b_4 U_c + b_5}$$

$$T_c = k_1 T_{af} \left(\frac{p_c}{p_{af}} \right)^{(\gamma-1)/\gamma}$$

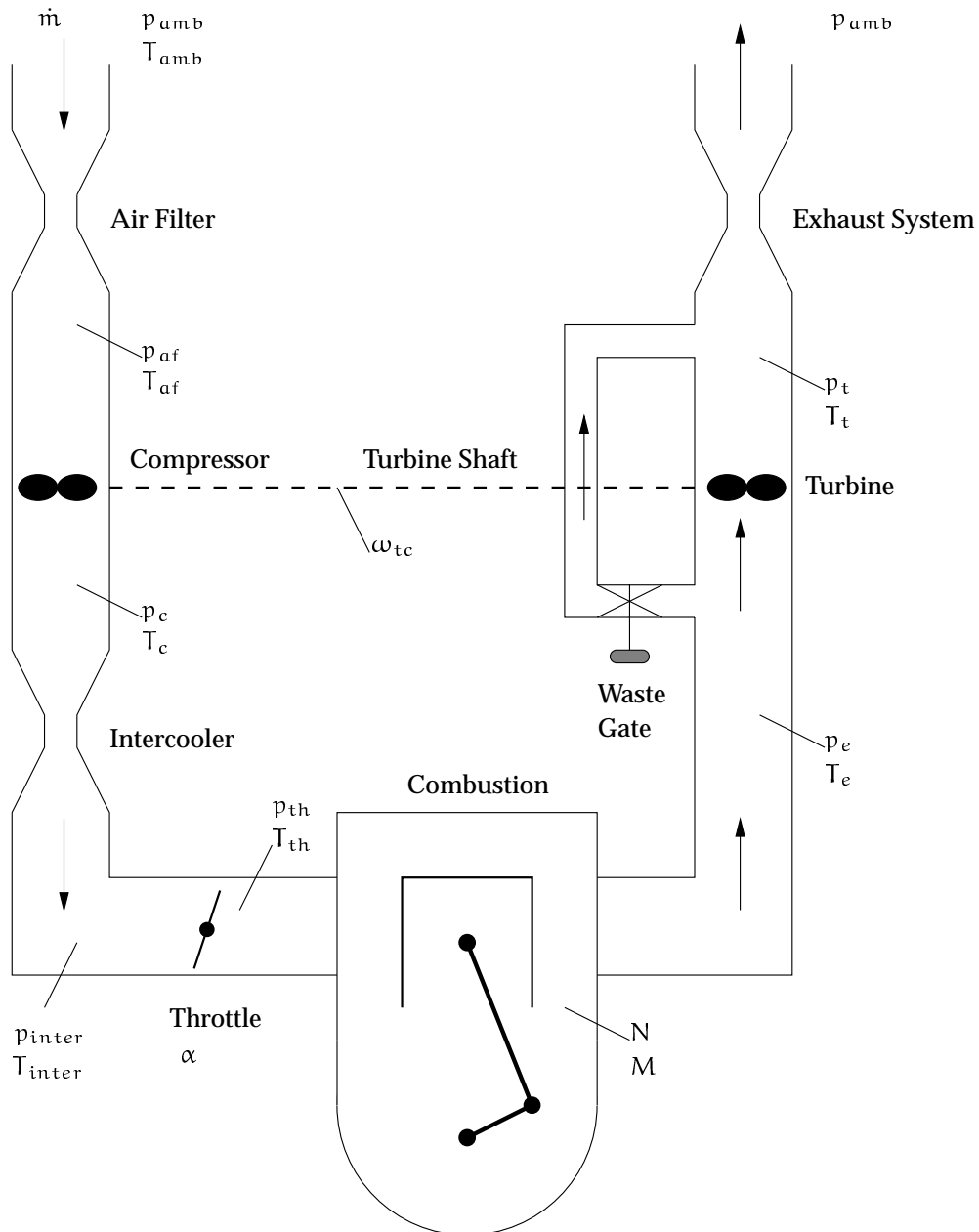


Figure 2.22 A schematic picture of a turbo charged engine. All the state variables in the simulation model are presented in the figure. The flow restrictions which cause the pressure differences in the engine are air filter, compressor, inter-cooler, throttle, combustion, turbine, waste gate and exhaust system. In addition to the state variables, some other quantities which are central in the modeling are included in the figure.

Chapter 3

Simulation of System Dynamics

Several experiments have been performed to establish the dominant time constant of the simulation model. The time constants of interest here are the filling dynamics of the volumes in the model and the turbine shaft speed dynamics. Occasions with faster time constants, such as the changes in mass flows, are modeled with static relationships. The changes in e.g. ambient temperature and ambient pressure are obviously slower than the dynamics of interest here and these properties are hence modeled as constants.

When doing a step response experiment, there are several characteristics related to the timescale that are interesting to measure. Two of these are the response time, T_r , and the settling time, T_s . T_r is the time needed for the output to proceed from 0.1 of its final value to 0.9 of its final value. T_s is defined as the smallest time, t , which satisfies $1 - p \leq y(t) \leq 1 + p$ for all $t > T_s$. $y(t)$ is the output and $p=5\%$. In this case $y(t)$ has the final value 1. These definitions of T_s and T_r come from [7].

The dynamics of the isolated dynamic elements are, to the greatest extent, governed by T_r , while the dynamics of the total model depend on T_s . T_r is often at least a factor ten faster than T_s . One obvious problem encountered when T_s is used as a measure of the dynamics of the model, is the fact that it depends on the properties of the waste gate. The model of the waste gate and the waste gate controller were discussed in Section 2.9.3 and it should be noted that the calculated controller parameters were somewhat arbitrary. The dynamics at high loads do therefore, unfortunately, depend on the choice of waste gate controller parameters. T_s should however give a good qualitative picture of the engine dynamics.

3.1 Subsystem Dynamics

It is interesting to see if there are any big differences in time constants between the sub models. Because, if the time constants vary a great deal the total time constant might in fact be governed by the slowest time constant in the model. The faster dynamics can then be seen as static properties which follow the slow dynamics perfectly. Fundamental difficulties, as the model is simulated, may also occur if the time constants vary a great deal (stiff problem).

As mentioned above, the time constants of the subsystems are set by T_r and for that reason it is important to know the magnitudes of T_r in the subsystems at various operating points. It is not altogether easy to determine T_r in the subsystems, as all dynamic elements in the model are influenced by each other.

Although one should note that the time constants of the filling dynamics of the different volumes (except the air filter) and the time constant of the turbine shaft speed have the same magnitude. The reason why the model still is not altogether easy to simulate might be the significantly faster dynamics of the air filter. The ratio between the slowest and the fastest time constant in the system is not greater than 100, so the system is not particularly stiff. It does however seem advantageous to use ODE-solvers, which are designed for stiff problems. Stiff differential equations are discussed more closely in Appendix A.1.4.

3.1.1 Filling Dynamics

The pressure dynamics is, as described previously in this chapter, modeled by using tanks that are filled and emptied. The total volume of the intake system and exhaust system has been divided into the following tanks:

- Air filter: $V_{af}=4 \text{ dm}^3$
- Compressor to intercooler: $V_c=5 \text{ dm}^3$
- Intercooler to throttle: $V_{inter}=5 \text{ dm}^3$
- Intake manifold: $V_{th}=2 \text{ dm}^3$
- Exhaust manifold: $V_e=2 \text{ dm}^3$
- Exhaust system: $V_{es}=10 \text{ dm}^3$

The volumes of the tanks ought to affect the dynamic properties of the engine in some way. It seems reasonable that a large volume has slower dynamics than a small volume. This hypothesis is confirmed by experiments on the model. In fact, T_r for a dynamic element turns out to be proportional to the volume of the corresponding tank.

In order to isolate the time constants of the filling dynamics, the turbine shaft dynamics were modeled as infinitely fast, i.e. changes in turbine shaft speed are

instantaneous. A throttle angle step experiment can be applied to reveal the dynamics of the volumes in the model. First of all the steady state turbine shaft speed was determined both before and after a step change in throttle angle was introduced. These values were noted. Secondly, the normal turbine shaft speed feed back was broken and replaced by a step change in turbine shaft speed. The initial and final values of the step were, of course, the initial steady state turbine shaft speed and the final turbine shaft speed, respectively.

This experiment was carried out for positive as well as negative step changes in throttle angle. The results of these tests are presented in Tables 3.1 and 3.2. It can be noted that the response times depend on whether the step change in throttle angle is positive or negative.

Engine Speed	Response Time T_r [s]					
N [RPM]	p_{af}	p_c	p_{inter}	p_{th}	p_e	p_t
1500	0.2	0.2	0.2	0.2	0.3	0.2
2500	0.2	0.2	0.2	0.2	0.2	0.2
3500	0.2	0.2	0.1	0.1	0.2	0.2
4500	0.2	0.2	0.1	0.1	0.2	0.1
5500	0.2	0.2	0.2	0.2	0.2	0.2

Table 3.1 Response times T_r for the filling dynamics. Step change in ω_{tc} and step change in α : $0.5 \rightarrow 0.8$ [rad].

Engine Speed	Response Time T_r [s]					
N [RPM]	p_{af}	p_c	p_{inter}	p_{th}	p_e	p_t
1500	0.2	0.2	0.2	0.2	0.3	0.2
2500	0.2	0.2	0.2	0.2	0.3	0.3
3500	0.02	0.3	0.3	0.2	0.2	0.2
4500	0.05	0.5	0.5	0.4	0.5	0.3
5500	0.05	0.4	0.4	0.7	0.5	0.4

Table 3.2 Response times T_r for the filling dynamics. Step change in ω_{tc} and step change in α : $0.8 \rightarrow 0.5$ [rad]. The time responses for negative step changes in throttle are similar to those obtained for positive step changes in Table 3.1.

3.2 Total Dynamics

The total time constant for all dynamic elements in the engine can be found through a fast change of the working point. The normal way to change the working conditions in a gasoline engine is to change the throttle angle. If this experiment is repeated at different engine speeds, we are likely to get rather good knowledge

of the engine speed dependency on the total time constant. The model was tested with both positive and negative step changes of the throttle angle and the results from these simulations are presented in Tables 3.3 through 3.6. It appears to be a discrepancy in both T_r and T_s between positive and negative step changes in throttle angle.

Engine Speed	Response Time T_r [s]						
N [RPM]	p_{af}	p_c	p_{inter}	p_{th}	p_e	p_t	ω_{tc}
1500	4.0	4.5	4.5	4.5	4.5	4.5	5.0
2500	0.04	0.1	0.01	0.1	0.01	0.1	0.06
3500	0.04	0.1	0.01	0.1	0.01	0.1	0.06
4500	0.05	0.1	0.01	0.1	0.01	0.1	0.05
5500	0.05	0.1	0.01	0.1	0.01	0.1	0.05

Table 3.3 Response times T_r for the total dynamics. Step change in α : $0.5 \rightarrow 0.8$ [rad]. The response times are particularly long at 1500 RPM, but seem to be nearly constant at higher engine speeds.

Engine Speed	Response Time T_r [s]						
N [RPM]	p_{af}	p_c	p_{inter}	p_{th}	p_e	p_t	ω_{tc}
1500	1.0	1.5	1.5	1.5	1.5	1.7	1.6
2500	0.02	1.3	1.4	1.4	0.02	0.05	0.04
3500	1.2	1.5	1.5	1.6	1.1	1.3	1.2
4500	0.05	0.7	0.7	0.8	0.01	0.10	0.10
5500	0.04	0.6	0.6	0.7	0.02	0.05	0.05

Table 3.4 Response times T_r for the total dynamics. Step change in α : $0.8 \rightarrow 0.5$ [rad]. The trend in response times is not as regular for this experiment as it was for the positive step change experiment. The dynamics does however get faster when the engine speed increases. The response times at 5500 RPM do not follow this general trend. One reason for this might be the waste gate controller, which is not optimized for such high loads.

Engine Speed	Settling Time T_s [s]						
N [RPM]	p_{af}	p_c	p_{inter}	p_{th}	p_e	p_t	ω_{tc}
1500	5.5	5.0	5.0	5.0	5.5	5.5	5.5
2500	0.4	0.8	0.8	0.9	0.8	0.5	0.9
3500	0.5	0.8	0.6	0.8	0.9	0.5	0.4
4500	0.4	0.8	0.5	0.8	0.5	0.4	0.4
5500	0.4	0.7	0.4	0.6	0.5	0.3	0.3

Table 3.5 Settling times T_s for the total dynamics. Step change in α : $0.5 \rightarrow 0.8$ [rad]. The settling times are, as expected, similar to the response times in Table 3.3.

Engine Speed	Settling Time T_s [s]						
N [RPM]	p_{af}	p_c	p_{inter}	p_{th}	p_e	p_t	ω_{tc}
1500	1.0	1.7	1.7	1.7	2.0	1.8	1.8
2500	1.8	1.9	2.0	2.0	1.8	1.8	1.9
3500	1.7	1.7	1.6	1.6	1.9	1.7	1.7
4500	1.2	1.2	1.2	1.2	1.4	1.2	1.3
5500	0.9	1.0	1.0	1.0	1.3	0.9	1.1

Table 3.6 Settling times T_s for the total dynamics. Step change in α : $0.8 \rightarrow 0.5$ [rad]. The settling times are, as expected, similar to the response times in Table 3.4.

Chapter 4

System Validation

In the following sections the simulation results are presented and compared with measurements on the real engine in the laboratory. The model is validated in terms of both static and dynamic properties. In the first case the measurements are made when all dynamic effects have died out. The engine dynamics are validated by using data from experiments where the throttle is subject to step changes, i.e. the system dynamics are validated with respect to step responses.

4.1 Stationary Validation

The most straightforward way to determine the quality of the model is probably to compare the modeled power output with measured power output for a certain throttle angle α . But, there are of course many other parameters of interest for the model validation, e.g. pressures, temperatures and mass flows. The models of these properties have been validated individually in Chapter 2, but it is also important to investigate how the different subsystems interact. The purpose of the validation is to point out both the good sub models and the sub models which need more modeling. Finally, the quality of the complete model can be established. All values compared here come from measurements under steady-state conditions, i.e. when all dynamic effects have died out.

It is desirable to measure as many quantities as possible in order to get a solid ground for the validation. The measurement system allows all state variables to be measured, i.e. six pressures and the turbine shaft speed. The mass flow through the engine is also measured since it is a central property in the engine model which is responsible for the pressure build up. In addition to the state variables and

mass flow the torque and temperatures have been measured. The results from experiments at five different engine speeds are shown in Tables 4.2 through 4.6. Note that the unit for the pressures is *kPa* in these tables. The temperature, T_{amb} , and the pressure, p_{amb} , in the laboratory were noted before the measurements started and stayed approximately constant during the measurements. The ambient conditions were $T_{amb} = 296\text{K}$ and $p_{amb} = 101.7\text{kPa}$. These values were used in the simulation model in order to get representative values for the environmental conditions in the simulations.

4.1.1 Description of the Experiments

Two different experiments were made on the simulation model to validate its stationary properties.

- The first experiment, called *Simulation 1*, is a straightforward comparison between the model and the engine in the laboratory. The inputs to the model are α , N , T_{amb} and p_{amb} , and all other parameters are noted.
- In the second experiment the measured turbine shaft speed is set to a constant value equal to the measured. By setting the turbine shaft speed to a constant value, the feed back inherent in the system, is broken. The experiments at constant turbine shaft speeds are referred to as *Simulation 2*.

The simulation results and measured data are presented in tabular form. Table 4.1 is a representative section of the validation tables and it displays the structure of the validation tables. *Error 1* and *Error 2* stand for the errors made by the model in Simulation 1 and Simulation 2, respectively. The errors are simply calculated as

$$\text{Error} = \frac{\text{Simulated value} - \text{Measured value}}{\text{Measured value}}$$

To save space in the tables, the units for the quantities in the tables do not always follow the standard nomenclature in the report. For convenience all units which appear in the tables are listed here: α [deg], pressures [kPa], ω_{tc} [rad/s], \dot{m} [kg/s], M [Nm] and temperatures [K].

4.1.2 Evaluation of Measurement and Simulation Data

The simulation results are presented in Tables 4.2 through 4.6 and are discussed here.

- From the values of ω_{tc} in the validation at $N=1000$ RPM (Table 4.2) and $N=1800$ RPM (Table 4.3) it is obvious that the model of the turbocharger does not work very well at low turbine shaft speeds (e.g. Error 1 in ω_{tc} in Table 4.2 at $\alpha = 2.1$ deg). An explanation to this shortcoming of the model is probably that the turbocharger data, from which the model is made, is restricted

$\alpha = 17.3$ deg	p_{af}	p_c	p_{inter}	p_{th}	p_e	p_{es}	ω_{tc}
Measurement	100.4	143.5	139.7	108.2	154.0	117.4	9568
Simulation 1	100.1	155.0	151.2	116.2	162.0	110.9	11418
Error 1 [%]	-0.3	8.0	8.2	7.4	5.2	-5.5	19.3
Simulation 2	100.5	135.9	133.1	102.8	166.7	109.0	9568
Error 2 [%]	0.1	-5.3	-4.7	-5.0	8.2	-7.2	0
	\dot{m}	M	T_{af}	T_c	T_{inter}	T_{th}	T_t
Measurement	0.0531	183	295	335	299	306	1037
Simulation 1	0.0640	218	296	354	305	305	966
Error 1 [%]	20.5	19.1	0.3	5.7	2.0	-0.3	-6.8
Simulation 2	0.0560	188	296	340	303	303	909
Error 2 [%]	5.5	2.7	0.3	1.5	1.3	-1.0	-12.3

Table 4.1 The table shows a part of the steady state validation at $N=2800$ RPM and $\alpha = 17.3$ deg.

to turbine shaft speeds over 8000 rad/s. The extrapolation capabilities of the model down to turbine shaft speeds under 3000 rad/s are therefore, as expected, quite bad.

- The simulated pressures before and after the compressor i.e. p_{af} and p_c do mostly agree well with the measurements (e.g. Error 1 in p_{af} and p_c in Table 4.3 at $\alpha = 20.5$ deg). The load on the compressor is therefore likely to be correct. The error in the simulated pressure after the turbine, p_t , is always smaller (with respect to sign) than the error in the simulated pressure before the turbine, p_e (e.g. Error 1 in p_e and p_t in Table 4.4 at $\alpha = 17.3$ deg). The driving torque on the turbine increases when p_e/p_t increases and the driving torque on the turbine will therefore be unreasonably high. The combination of correct load on the compressor and too high driving torque on the turbine will result in too high turbine shaft speed (e.g. Error 1 in ω_{tc} in Table 4.4 at $\alpha = 17.3$ deg).
- The pressure after the throttle, p_{th} , is crucial for the engine as it strongly influences the mass flow into the cylinders and hence the output power from the engine. The model seems to capture this pressure well at all engine speeds. There is also good agreement between measured data and the simulations at most throttle angles, α (e.g. Error 1 in p_{th} in Table 4.3 at $\alpha = 29.8$ deg). The exception is the smallest throttle angle for every engine speed which agrees less with measured data (e.g. Error 1 in p_{th} in Table 4.3 at $\alpha = 4.8$ deg).
- A central quantity in the engine model is the mass flow, \dot{m} , through the throttle. The modeled mass flow is generally a bit too high (e.g. Error 1 in \dot{m} in Table 4.6 at $\alpha = 28.7$ deg). It has been modeled as a function of p_{inter} , p_{th} ,

α and T_{inter} . The error in \dot{m} is mostly bigger than the corresponding errors in p_{inter} and p_{th} (e.g. Error 1 in p_{inter} and p_{th} in Table 4.6 at $\alpha = 28.7$ deg). According to the validation plot in Figure 2.7 the mass flow model of the throttle works well. The errors in \dot{m} may be caused by problems in measuring the throttle angle properly.

- The pressure after the intercooler, p_{inter} , follows the pressure after the compressor. It can be noted that there is very good agreement between the errors in p_c and p_{inter} (e.g. Error 1 in p_c and p_{inter} in Table 4.5 at $\alpha = 22.5$ deg); this indicates that almost no errors are added in the intercooler model.
- The largest addition of errors in the pressures arise in the compressor and the turbine. This is obvious if Error 1 is compared for p_{af} , p_c , p_e and p_t in e.g. Table 4.5 at $\alpha = 22.5$ deg. These additional errors do probably come from the turbocharger model and the model of the exhaust system. The model of p_t works well at low loads, but gives too low values at high loads.
- It is clear, from the errors in the output torque M , that the model of the combustion is not perfect (e.g. Error 1 in M in Table 4.4 at $\alpha = 17.3$ deg). The reason for this is probably deficiencies in the look-up tables for the volumetric efficiency and the combustion efficiency. This problem may be solved if new look-up tables are made from engine measurements at a large number of operating points. M is a parameter in the model of the exhaust manifold temperature, T_e , and therefore errors in M must propagate to the exhaust gas side of the engine. It has not been possible to measure T_e , so it is difficult to tell how severe the error propagation from M is.
- All temperature models, except for T_t (e.g. Error 1 in T_t in Table 4.4 at $\alpha = 7.2$ deg), are satisfactory. There is uncertainty whether the larger errors in T_t depend on model errors or measurement errors. The temperature sensor for T_t is namely stuck in the the exhaust tube and it is therefore impossible to inspect it. We did not have a chance to measure more than one temperature on the exhaust side of the engine. Since the measurements of T_t might be erroneous, the temperature models of the exhaust gases might still be correct.

In future extensions of this study it is important to verify all models further in order to eliminate sources of errors. Most models seem to be good, but according to the validation discussion above the models of the turbocharger, throttle and torque are likely to be the main causes of errors. The model of the waste gate is another possible source of errors.

4.2 Dynamic Validation

To make a good and useful simulation model it must of course be compared with the engine in the laboratory. The dynamic qualities of the model can be established

from e.g. step experiments. Step changes in throttle angle provide a straightforward method to get a good picture of the engine dynamics. The stationary values of the model were validated in the previous section and therefore solely dynamic properties are validated here.

In a simulation tool, like Simulink, it is possible to make extremely fast changes in throttle angle. In a real engine, the slope of the step is limited by the power of the throttle servo. A typical throttle step takes about 0.3 seconds from initial level to final level. Due to this physical restriction a, physically reasonable, flat step was used in the simulations, in order to get comparable results.

The step responses are given in Figures 4.1 through 4.4. These four plots show experiments at 1300 RPM and 2300 RPM for both low loads and high loads. According to these figures the model seems to capture the dynamic characteristics well at 2300 RPM. The agreement is slightly less at 1300 RPM. Hence, the model seems to work better at 2300 RPM than at 1300 RPM and it is therefore likely to work well at higher engine speeds than 2300 RPM as well.

In all plots of p_e and ω_{tc} there is a time delay between the simulated and measured values. This indicates that it should be beneficial with some type of engine speed dependent time delay in the combustion model.

The oscillations in p_c which can be seen in Equation (4.4) are due to the waste gate controller. If the gain in the PI-controller is lowered the oscillations will be smaller, but this method might on the other hand result in a too slow controller which does not manage to keep p_c under its reference value. Perhaps other controller designs, such as model based controllers, can solve this problem, but it has not been possible to test any of these more advanced design methods as we have not had access to an explicit state space model of the system. Construction of an explicit state space model and tests of model based control designs are however possible follow-ups to this study.

$\alpha = 2.1 \text{ deg}$	p_{af}	p_c	p_{inter}	p_{th}	p_e	p_t	ω_{tc}
Measurement	101.7	102.6	101.6	46.5	103.0	101.9	1276
Simulation 1	101.7	102.9	102.9	51.9	104.2	102.2	3911
Error 1 [%]	0.0	0.3	1.3	11.6	1.2	0.3	206.5
Simulation 2	101.7	86.4	86.4	43.6	103.5	102.1	1276
Error 2 [%]	0.0	-15.8	-15.0	-6.2	0.5	0.2	0
	\dot{m}	M	T_{af}	T_c	T_{inter}	T_{th}	T_t
Measurement	0.0069	46.6	296	304	295	318	586
Simulation 1	0.0087	51.4	296	313	297	297	583
Error 1 [%]	26.1	10.3	0.0	3.0	0.7	-6.6	1.2
Simulation 2	0.0073	32.2	296	296	296	296	587
Error 2 [%]	5.8	-30.9	0.0	-2.6	0.3	-6.9	0.2
$\alpha = 4.3 \text{ deg}$	p_{af}	p_c	p_{inter}	p_{th}	p_e	p_t	ω_{tc}
Measurement	101.7	104.8	103.8	66.2	104.4	102.2	2551
Simulation 1	101.6	104.1	104.0	68.2	106.3	102.5	4225
Error 1 [%]	-0.1	-0.7	0.2	3.0	1.8	0.3	65.6
Simulation 2	101.7	93.1	93.0	62.0	105.4	102.3	2551
Error 2 [%]	0.0	-11.2	-10.4	-6.3	1.0	0.1	0
	\dot{m}	M	T_{af}	T_c	T_{inter}	T_{th}	T_t
Measurement	0.0101	87.2	296	305	295	315	646
Simulation 1	0.0123	96.6	296	315	298	298	615
Error 1 [%]	21.8	10.8	0.0	3.3	1.0	-5.4	-4.8
Simulation 2	0.0109	77.8	296	296	296	296	605
Error 2 [%]	7.9	-10.8	0.0	-3.0	0.3	-6.0	-6.3
$\alpha = 8.2 \text{ deg}$	p_{af}	p_c	p_{inter}	p_{th}	p_e	p_t	ω_{tc}
Measurement	101.7	110.4	109.3	90.4	107.2	102.9	4255
Simulation 1	101.6	106.2	106.0	88.9	109.5	102.8	4676
Error 1 [%]	-0.1	-3.8	-3.0	-1.7	2.1	-0.1	9.9
Simulation 2	101.6	103.2	103.0	86.4	109.1	102.8	4255
Error 2 [%]	-0.1	-6.5	-5.8	-4.4	1.8	-0.1	0
	\dot{m}	M	T_{af}	T_c	T_{inter}	T_{th}	T_t
Measurement	0.0143	134	295	307	294	311	734
Simulation 1	0.0166	144	296	316	298	298	649
Error 1 [%]	16.1	7.5	0.3	2.9	1.4	-4.2	-11.6
Simulation 2	0.0161	140	296	314	298	298	646
Error 2 [%]	12.6	4.5	0.3	2.3	1.4	-4.2	-12.0
$\alpha = 15.5 \text{ deg}$	p_{af}	p_c	p_{inter}	p_{th}	p_e	p_t	ω_{tc}
Measurement	101.6	116.3	114.9	108.9	110.5	104.0	5485
Simulation 1	101.6	107.9	107.6	102.8	112.0	103.1	5010
Error 1 [%]	0.0	-7.2	-6.4	-5.6	1.4	-0.9	-8.7
Simulation 2	101.5	111.4	111.1	106.1	112.8	103.2	5485
Error 2 [%]	-0.1	-4.2	-3.3	-2.6	2.1	-0.8	0
	\dot{m}	M	T_{af}	T_c	T_{inter}	T_{th}	T_t
Measurement	0.0185	167	296	313	295	308	829
Simulation 1	0.0194	170	296	318	298	298	672
Error 1 [%]	4.9	1.8	0.0	1.6	1.0	-3.2	-18.9
Simulation 2	0.0202	178	296	321	298	298	680
Error 2 [%]	9.2	6.6	0.0	2.6	1.0	-3.2	-18.0

Table 4.2 Steady state validation at $N=1000 \text{ RPM}$

$\alpha = 4.8 \text{ deg}$	p_{af}	p_c	p_{inter}	p_{th}	p_e	p_t	ω_{tc}
Measurement	101.7	104.5	103.5	41.3	105.5	102.4	2469
Simulation 1	101.6	105.1	105.0	46.5	107.5	102.7	4424
Error 1 [%]	-0.1	0.6	1.4	12.6	1.9	0.3	79.2
Simulation 2	101.6	92.3	92.2	41.0	106.3	102.5	2469
Error 2 [%]	-0.1	-11.7	-10.9	-0.7	0.8	0.1	0
	\dot{m}	M	T_{af}	T_c	T_{inter}	T_{th}	T_t
Measurement	0.0110	38.0	296	305	295	313	739
Simulation 1	0.0139	39.4	296	315	298	298	691
Error 1 [%]	26.4	3.7	0.0	3.3	1.0	-4.8	-6.5
Simulation 2	0.0122	23.9	296	296	296	296	685
Error 2 [%]	10.9	-37.1	0.0	-3.0	0.3	-5.4	-7.3
$\alpha = 10.1 \text{ deg}$	p_{af}	p_c	p_{inter}	p_{th}	p_e	p_t	ω_{tc}
Measurement	101.5	122.6	121.1	83.7	119.7	104.8	6577
Simulation 1	101.4	116.5	115.9	82.4	120.8	104.1	6393
Error 1 [%]	-0.1	-5.0	-4.6	-1.6	0.9	-0.7	-2.8
Simulation 2	101.4	118.0	117.4	83.4	121.2	104.2	6577
Error 2 [%]	-0.1	-3.8	-3.1	-0.4	1.3	-0.6	0
	\dot{m}	M	T_{af}	T_c	T_{inter}	T_{th}	T_t
Measurement	0.0243	128	296	317	296	308	858
Simulation 1	0.0275	132	296	325	299	299	750
Error 1 [%]	13.2	3.4	0.0	2.5	1.0	-2.9	-12.6
Simulation 2	0.0278	134	296	326	299	299	752
Error 2 [%]	14.4	4.7	0.0	2.8	1.0	-2.9	-12.4
$\alpha = 20.5 \text{ deg}$	p_{af}	p_c	p_{inter}	p_{th}	p_e	p_t	ω_{tc}
Measurement	100.9	151.8	149.0	138.0	144.4	111.2	10121
Simulation 1	100.7	155.0	152.6	140.9	153.9	108.3	10867
Error 1 [%]	-0.2	2.1	2.4	2.1	6.6	-2.6	7.4
Simulation 2	100.8	146.7	144.6	133.8	152.6	107.6	10121
Error 2 [%]	-0.1	-3.4	-3.0	-3.0	5.7	-3.2	0
	\dot{m}	M	T_{af}	T_c	T_{inter}	T_{th}	T_t
Measurement	0.0442	238	296	343	300	307	994
Simulation 1	0.0516	275	296	353	304	304	932
Error 1 [%]	16.7	15.5	0.0	2.9	1.3	-1.0	-6.2
Simulation 2	0.0485	256	296	348	303	303	897
Error 2 [%]	9.7	7.6	0.0	1.5	1.0	-1.3	-9.8
$\alpha = 29.8 \text{ deg}$	p_{af}	p_c	p_{inter}	p_{th}	p_e	p_t	ω_{tc}
Measurement	100.7	157.4	154.1	150.3	151.3	114.3	10720
Simulation 1	100.6	155.0	152.2	148.1	155.3	109.1	11011
Error 1 [%]	-0.1	-1.5	-1.2	-1.5	2.6	-4.5	2.7
Simulation 2	100.6	151.7	149.1	145.1	162.1	108.7	10720
Error 2 [%]	-0.1	-3.6	-3.2	-3.5	7.1	-4.9	0
	\dot{m}	M	T_{af}	T_c	T_{inter}	T_{th}	T_t
Measurement	0.0481	256	297	354	304	310	1047
Simulation 1	0.0549	295	296	353	304	304	972
Error 1 [%]	14.1	15.2	-0.3	-0.3	0.0	-1.9	-7.2
Simulation 2	0.0536	287	296	351	304	304	949
Error 2 [%]	11.4	12.1	-0.3	-0.8	0.0	-1.9	-9.4

Table 4.3 Steady state validation at $N=1800 \text{ RPM}$

$\alpha = 7.2 \text{ deg}$	p_{af}	p_c	p_{inter}	p_{th}	p_e	p_t	ω_{tc}
Measurement	101.5	115.3	113.9	48.6	115.1	104.4	5337
Simulation 1	101.5	109.1	108.8	43.9	112.8	103.3	5197
Error 1 [%]	0.0	-5.4	-4.5	-9.7	-2.0	-1.1	-2.6
Simulation 2	101.5	110.2	109.9	44.3	112.9	103.4	5337
Error 2 [%]	0.0	-4.4	-3.5	-8.8	-1.9	-1.0	0
	\dot{m}	M	T_{af}	T_c	T_{inter}	T_{th}	T_t
Measurement	0.0205	48.8	294	311	294	307	880
Simulation 1	0.0200	28.3	296	319	298	298	776
Error 1 [%]	-2.4	-42.0	0.7	2.6	1.4	-2.9	-11.8
Simulation 2	0.0202	29.6	296	320	298	298	777
Error 2 [%]	-1.5	-39.3	0.7	2.9	1.4	-2.9	-11.7
$\alpha = 17.3 \text{ deg}$	p_{af}	p_c	p_{inter}	p_{th}	p_e	p_t	ω_{tc}
Measurement	100.4	143.5	139.7	108.2	154.0	117.4	9568
Simulation 1	100.1	155.0	151.2	116.2	162.0	110.9	11418
Error 1 [%]	-0.3	8.0	8.2	7.4	5.2	-5.5	19.3
Simulation 2	100.5	135.9	133.1	102.8	166.7	109.0	9568
Error 2 [%]	0.1	-5.3	-4.7	-5.0	8.2	-7.2	0
	\dot{m}	M	T_{af}	T_c	T_{inter}	T_{th}	T_t
Measurement	0.0531	183	295	335	299	306	1037
Simulation 1	0.0640	218	296	354	305	305	966
Error 1 [%]	20.5	19.1	0.3	5.7	2.0	-0.3	-6.8
Simulation 2	0.0560	188	296	340	303	303	909
Error 2 [%]	5.5	2.7	0.3	1.5	1.3	-1.0	-12.3
$\alpha = 31.7 \text{ deg}$	p_{af}	p_c	p_{inter}	p_{th}	p_e	p_t	ω_{tc}
Measurement	99.4	152.1	146.5	139.1	177.5	129.6	10663
Simulation 1	99.3	155.0	149.1	141.4	172.0	115.3	12153
Error 1 [%]	-0.1	1.9	1.8	1.7	-3.1	-11.0	14.0
Simulation 2	99.7	140.1	135.5	128.6	202.1	112.8	10663
Error 2 [%]	0.3	-7.9	-7.5	-7.5	13.9	-13.0	0
	\dot{m}	M	T_{af}	T_c	T_{inter}	T_{th}	T_t
Measurement	0.0704	251	296	343	303	309	1112
Simulation 1	0.0801	282	296	355	307	307	1092
Error 1 [%]	13.8	12.4	0.0	3.5	1.3	-0.6	-1.8
Simulation 2	0.0722	250	296	344	304	304	998
Error 2 [%]	2.6	-0.4	0.0	0.3	0.3	-1.6	-10.3
$\alpha = 41.6 \text{ deg}$	p_{af}	p_c	p_{inter}	p_{th}	p_e	p_t	ω_{tc}
Measurement	99.1	157.4	151.2	148.7	187.0	133.4	11190
Simulation 1	99.1	155.0	148.7	145.4	173.7	116.1	12272
Error 1 [%]	0.0	-1.5	-1.7	-2.2	-7.1	-13.0	9.7
Simulation 2	99.5	144.1	133.8	135.7	213.2	114.1	11190
Error 2 [%]	0.4	-8.4	-8.2	-8.7	14.0	-14.5	0
	\dot{m}	M	T_{af}	T_c	T_{inter}	T_{th}	T_t
Measurement	0.0747	266	297	350	306	312	1131
Simulation 1	0.0827	292	296	355	307	307	1116
Error 1 [%]	10.7	9.8	-0.3	1.4	0.3	-1.6	-1.3
Simulation 2	0.0767	268	296	347	305	305	1028
Error 2 [%]	2.7	0.8	-0.3	-0.9	-0.3	-2.2	-9.1

Table 4.4 Steady state validation at $N=2800 \text{ RPM}$

$\alpha = 6.6 \text{ deg}$	p_{af}	p_c	p_{inter}	p_{th}	p_e	p_t	ω_{tc}
Measurement	101.5	116.4	115.2	38.4	116.7	104.7	5646
Simulation 1	101.6	108.5	108.2	33.3	111.4	103.3	5045
Error 1 [%]	0.1	-6.8	-6.1	-13.3	-4.5	-1.3	-10.6
Simulation 2	101.6	113.1	112.8	34.5	112.1	103.3	5646
Error 2 [%]	0.1	-2.8	-2.1	-10.2	-3.9	-1.3	0
	\dot{m}	M	T_{af}	T_c	T_{inter}	T_{th}	T_t
Measurement	0.0205	18.6	297	319	298	312	947
Simulation 1	0.0184	-12.0	296	318	298	298	825
Error 1 [%]	-10.2	-164.5	-0.3	-0.3	0.0	-4.5	-12.9
Simulation 2	0.0192	-9.6	296	322	298	298	826
Error 2 [%]	-6.3	-151.6	-0.3	0.9	0.0	-4.5	-12.8
$\alpha = 12.8 \text{ deg}$	p_{af}	p_c	p_{inter}	p_{th}	p_e	p_t	ω_{tc}
Measurement	100.6	141.6	138.2	81.0	151.6	116.8	9422
Simulation 1	100.7	155.0	152.6	76.0	154.3	108.1	10851
Error 1 [%]	0.1	9.5	10.4	-6.2	1.8	-7.4	15.2
Simulation 2	100.9	139.3	137.4	70.0	148.5	107.1	9422
Error 2 [%]	0.3	-1.6	-0.6	-13.6	-2.0	-8.3	0
	\dot{m}	M	T_{af}	T_c	T_{inter}	T_{th}	T_t
Measurement	0.0507	112	297	337	300	308	1056
Simulation 1	0.0513	109	296	353	304	304	904
Error 1 [%]	1.2	-2.7	-0.3	4.7	1.3	-1.3	-14.4
Simulation 2	0.0461	90.9	296	342	302	302	886
Error 2 [%]	-9.1	-18.8	-0.3	1.5	0.7	-1.9	-16.1
$\alpha = 22.5 \text{ deg}$	p_{af}	p_c	p_{inter}	p_{th}	p_e	p_t	ω_{tc}
Measurement	98.8	146.8	140.0	113.4	183.5	136.2	10540
Simulation 1	98.8	155.0	147.9	116.5	178.6	117.1	12494
Error 1 [%]	0.0	5.6	5.6	2.7	-2.7	-14.0	18.5
Simulation 2	99.5	136.0	130.8	103.2	213.5	113.9	10540
Error 2 [%]	0.7	-7.4	-6.6	-9.0	16.3	-16.4	0
	\dot{m}	M	T_{af}	T_c	T_{inter}	T_{th}	T_t
Measurement	0.0786	192	300	344	306	313	1146
Simulation 1	0.0875	216	296	355	307	307	1072
Error 1 [%]	11.3	12.5	-1.3	3.2	0.3	-1.9	-6.5
Simulation 2	0.0770	187	296	342	304	304	987
Error 2 [%]	-2.0	-2.6	-1.3	-0.6	-0.7	-2.9	-13.9
$\alpha = 29.4 \text{ deg}$	p_{af}	p_c	p_{inter}	p_{th}	p_e	p_t	ω_{tc}
Measurement	97.8	153.1	144.5	131.5	205.7	147.7	11501
Simulation 1	98.0	155.0	146.0	129.9	187.7	120.7	13029
Error 1 [%]	0.2	1.2	1.0	-1.2	-8.8	-18.3	13.3
Simulation 2	98.7	140.4	133.1	118.6	247.3	117.4	11501
Error 2 [%]	0.9	-8.3	-7.9	-9.8	-20.2	-20.5	0
	\dot{m}	M	T_{af}	T_c	T_{inter}	T_{th}	T_t
Measurement	0.0916	229	302	351	310	316	1171
Simulation 1	0.0988	247	296	356	309	309	1138
Error 1 [%]	7.9	7.9	-2.0	1.4	-0.3	-2.2	-2.8
Simulation 2	0.0898	222	296	345	306	306	1037
Error 2 [%]	-2.0	-3.1	-2.0	-1.7	-1.3	-3.2	-11.4

Table 4.5 Steady state validation at $N=3800 \text{ RPM}$

$\alpha = 9.0 \text{ deg}$	p_{af}	p_c	p_{inter}	p_{th}	p_e	p_t	ω_{tc}
Measurement	101.2	129.4	127.7	40.4	127.4	106.7	7564
Simulation 1	101.4	117.9	117.3	39.7	120.2	104.3	6510
Error 1 [%]	0.2	-8.9	-8.1	-1.7	-5.7	-2.2	-13.9
Simulation 2	101.4	127.1	126.4	42.2	122.7	104.6	7564
Error 2 [%]	0.2	-1.8	-1.0	4.5	-3.7	-2.8	0
	\dot{m}	M	T_{af}	T_c	T_{inter}	T_{th}	T_t
Measurement	0.0272	17.4	296	327	296	307	986
Simulation 1	0.0267	-8.9	296	326	299	299	877
Error 1 [%]	-1.8	-151.1	0.0	-0.3	1.0	-2.6	-11.1
Simulation 2	0.0288	-1.3	296	333	300	300	881
Error 2 [%]	5.9	-101.7	0.0	1.8	1.4	-2.3	-10.6
$\alpha = 16.9 \text{ deg}$	p_{af}	p_c	p_{inter}	p_{th}	p_e	p_t	ω_{tc}
Measurement	99.3	143.8	138.0	84.5	170.9	131.0	10036
Simulation 1	99.8	155.0	150.3	82.5	167.0	112.6	11755
Error 1 [%]	0.5	7.8	8.9	-2.4	-2.3	-14.0	17.1
Simulation 2	100.2	137.4	133.8	75.0	182.3	110.7	10036
Error 2 [%]	0.9	-4.5	-3.0	-11.2	6.7	-15.5	0
	\dot{m}	M	T_{af}	T_c	T_{inter}	T_{th}	T_t
Measurement	0.0689	118	300	341	304	311	1146
Simulation 1	0.0715	117	296	354	306	306	992
Error 1 [%]	3.8	-0.8	-1.3	3.8	0.7	-1.6	-13.4
Simulation 2	0.0636	99.2	296	342	303	303	950
Error 2 [%]	-7.7	-15.9	-1.3	0.3	-0.3	-2.6	-17.1
$\alpha = 28.7 \text{ deg}$	p_{af}	p_c	p_{inter}	p_{th}	p_e	p_t	ω_{tc}
Measurement	96.6	147.9	137.1	116.9	214.9	156.9	11747
Simulation 1	97.0	155.0	143.3	118.7	200.9	125.1	13677
Error 1 [%]	0.4	4.8	4.5	1.5	-6.5	-20.3	16.4
Simulation 2	97.9	137.5	128.5	106.9	276.7	120.4	11747
Error 2 [%]	1.3	-7.0	-6.3	-8.6	28.8	-23.3	0
	\dot{m}	M	T_{af}	T_c	T_{inter}	T_{th}	T_t
Measurement	0.1025	192	304	352	312	319	1170
Simulation 1	0.1122	212	296	357	310	310	1161
Error 1 [%]	9.5	10.4	-2.6	1.4	-0.6	-2.8	-0.8
Simulation 2	0.0999	185	296	344	307	307	1049
Error 2 [%]	-2.5	-3.6	-2.6	-2.3	-1.6	-3.8	-10.3
$\alpha = 46.7 \text{ deg}$	p_{af}	p_c	p_{inter}	p_{th}	p_e	p_t	ω_{tc}
Measurement	94.9	150.8	137.1	132.2	242.4	171.4	12711
Simulation 1	95.5	155.0	139.5	133.5	219.0	131.7	14510
Error 1 [%]	0.6	2.8	1.8	1.0	-9.5	-23.2	14.2
Simulation 2	96.6	139.3	127.0	121.7	331.4	125.9	12711
Error 2 [%]	1.8	-7.6	-7.4	-7.9	36.7	-26.5	0
	\dot{m}	M	T_{af}	T_c	T_{inter}	T_{th}	T_t
Measurement	0.1172	218	304	358	316	322	1142
Simulation 1	0.1290	249	296	359	312	312	1248
Error 1 [%]	10.1	14.2	-2.6	0.3	-1.3	-3.1	9.3
Simulation 2	0.1164	221	296	347	308	308	1104
Error 2 [%]	-0.7	1.4	-2.6	-3.1	-2.5	-4.3	-3.3

Table 4.6 Steady state validation at $N=4800 \text{ RPM}$

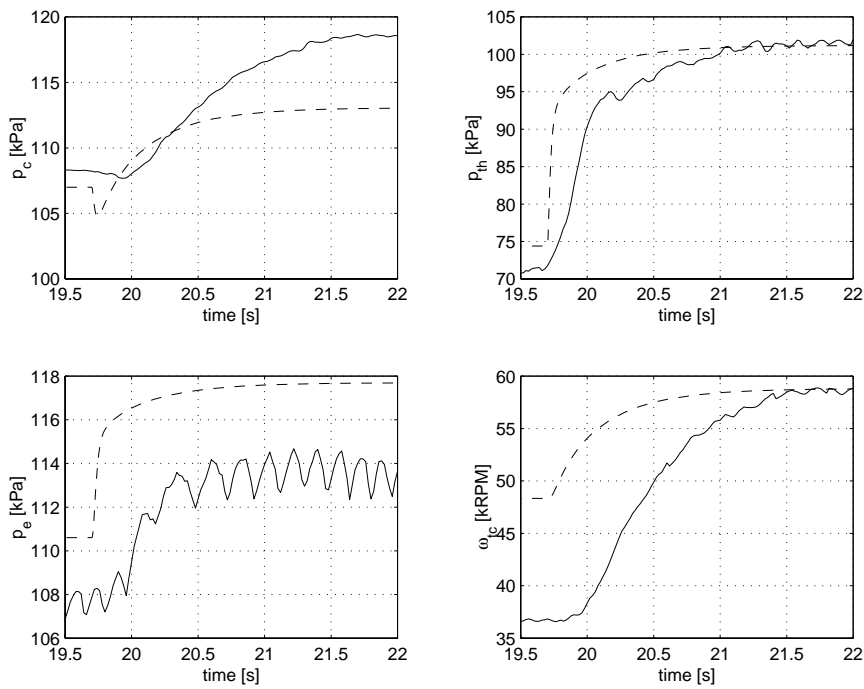


Figure 4.1 Step responses at 1300 RPM. The solid lines denote measured data and the dashed lines stand for simulated values. The throttle step starts at 19.7 s and the throttle angle goes from 8.0 deg to 13.0 deg

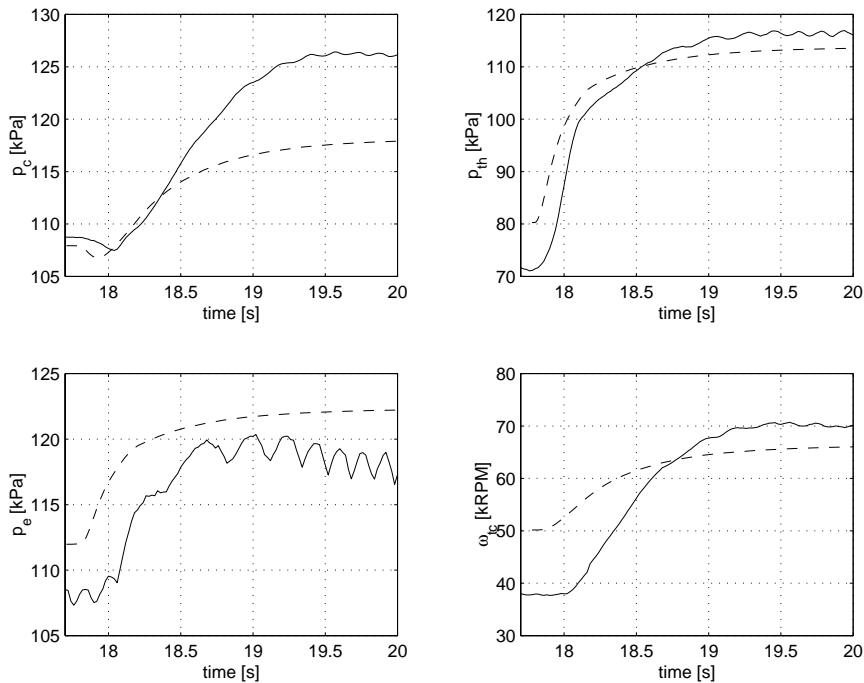


Figure 4.2 Step responses at 1300 RPM. The solid lines denote measured data and the dashed lines stand for simulated values. The throttle step starts at 17.8 s and the throttle angle goes from 8.0 deg to 22.0 deg

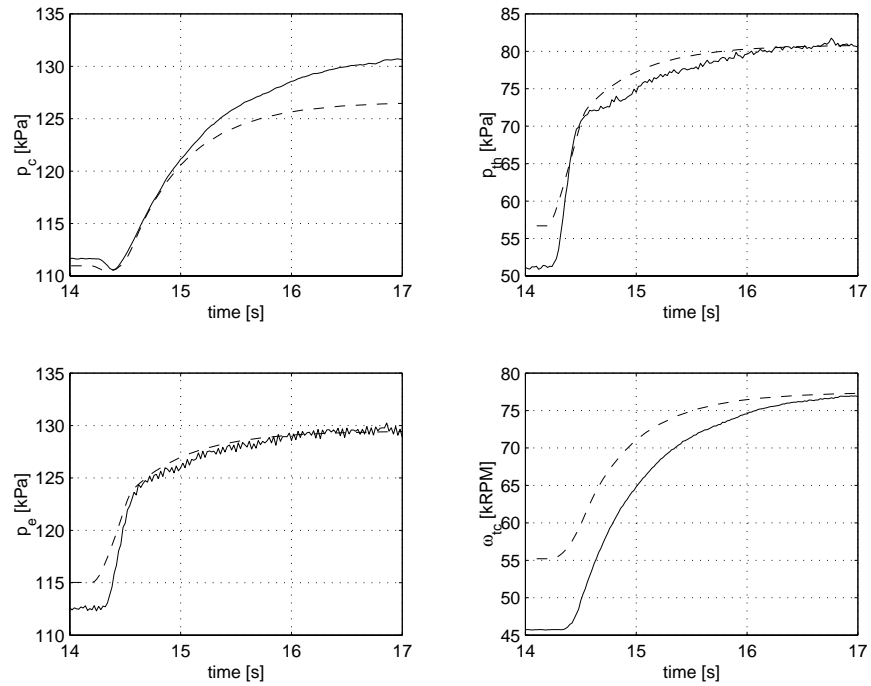


Figure 4.3 Step response at 2300 RPM. The solid lines denote measured data and the dashed lines stand for simulated values. The throttle step starts at 14.2 s and the throttle angle goes from 8.0 deg to 12.0 deg.

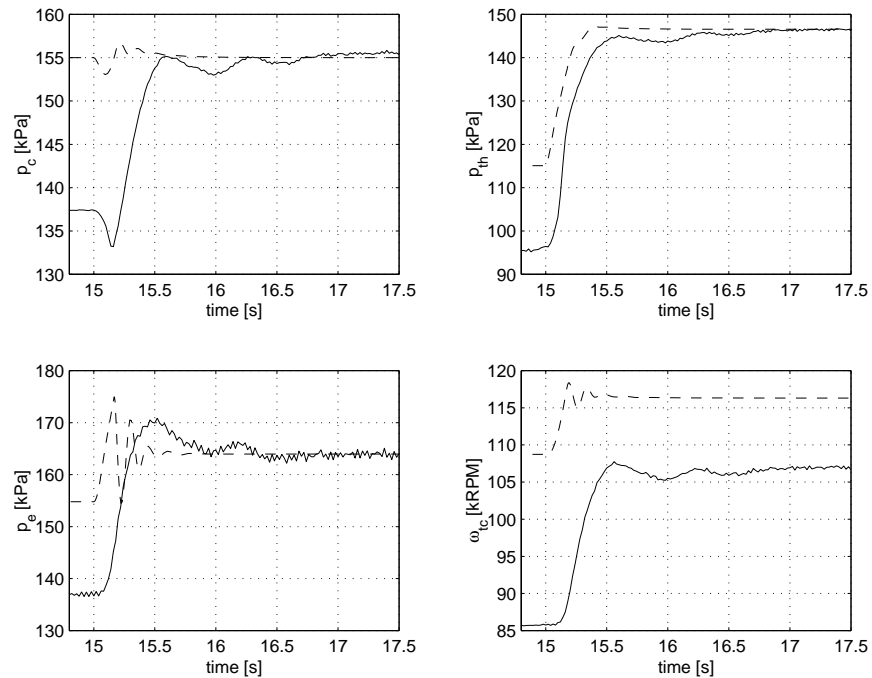


Figure 4.4 Step response at 2300 RPM. The solid lines denote measured data and the dashed lines stand for simulated values. The throttle step starts at 15.0 s and the throttle angle goes from 14.5 deg to 35.0 deg.

Chapter 5

Summary

The aim with this thesis project has been to develop a simulation model which can be used for control design and diagnosis purposes. This chapter is intended to highlight both good points of the model and areas which need to be studied in further detail. In Chapter 4 the quantitative analysis of the model is done and therefore mainly general qualitative aspects of the model will be discussed here.

5.1 Accomplishments

The primary purpose was to find a model which could be simulated in Simulink. The core of the model is the turbo charger equations from [5] which are straightforward and generally applicable. These equations are presented in Section 2.9. Starting with these turbo charger equations and the previous work by [2] models for the other engine parts have been constructed. All the equations in the model have been derived by combining physical modeling and black box modeling. This type of modeling is usually called grey box modeling. As mentioned above some models come from [5], [2] and [6] while this work has contributed with a few other new models of the subsystems. The new models are:

- Mass flow model of the turbine, Equation (2.33)
- Efficiency model of the turbine, Equation (2.34)
- Temperature model of the turbine, Equation (2.36)
- Mass flow model of the compressor, Equation (2.37)

- Temperature model of the compressor, Equation (2.39)
- Mass flow model of the exhaust system, Equation (2.28)
- Temperature model of the outlet manifold, Equation (2.26)

Finally the models of all subsystems were implemented in Simulink.

Every block in Simulink represents a well defined part of the engine. The obvious advantage with this approach is the fact that the blocks easily can be replaced, if a better model is found for some component of the engine. A logical block structure makes it also easier for a person who has not seen the model before to get used to it.

From the validation in Chapter 4 it is clear that the model captures the behavior of both dynamic and stationary experiments well. It is, as expected, more difficult to get an exact agreement between the simulation model and measured data. Some further development of the sub models needs to be done to make the model really useful for predictive purposes.

5.2 Future Challenges

Nevertheless, the overall model structure seems to be good and it should be used in future modeling projects. It would be interesting to implement the model in some other simulation environment to see if there will be any major changes in simulation times and simulation accuracy.

A severe drawback with Simulink is the fact that it can not produce an explicit state space model. Many interesting properties, such as sensitivity and robustness for disturbances and model errors, could be calculated if an explicit state space model was available. To model, using *Dymola* or *Modelica* would solve this problem as they are able to give explicit expressions of the state space model.

Another application for the state space model is to analyze stationary points in the solution. This is an interesting area to look at in more detail, as there is a chance that the solutions to the simulation equations only reach a finite number of stationary solutions, although the model parameters can be changed infinitely. A follow-up to this thesis project can study these stationary points and analyze the parameter errors.

Bibliography

- [1] Bilal M. Ayyub and Richard H. McCuen. *Numerical Methods for Engineers*. Prentice-Hall, 1996. ISBN 0-13-337361-4.
- [2] J. Bergström and J. Brugård. *Modeling of a Turbo Charged Spark Ignited Engine*. Linköping Institute of Technology, 1999.
- [3] Lars Eldén and Linde Wittmeyer-Koch. *Numerisk analys - en introduktion*. Studentlitteratur, 1992. ISBN 91-44-25652-3.
- [4] T. Glad, S. Gunnarsson, L. Ljung, and T. McKelvey. *Digital styrning kurskompendium*. Linköping Institute of Technology, 1999.
- [5] L. Guzzella and A. Amstutz. Control of diesel engines. *IEEE Control Systems*, October 1998.
- [6] John B. Heywood. *Internal Combustion Engine Fundamentals*. McGraw-Hill, 1988. ISBN 0-07-100499-8.
- [7] Lennart Ljung and Torkel Glad. *Reglerteknik - grundläggande teori*. Studentlitteratur, Lund, 1989. ISBN 91-44-17892-1.
- [8] Lennart Ljung and Torkel Glad. *Modellbygge och simulering*. Studentlitteratur, Lund, 1991. ISBN 91-44-31871-5.
- [9] K. Newton, W. Steeds, and T.K. Garret. *The Motor Vehicle*. Society of Automotive Engineers (SAE), 1996. ISBN 1-56091-898-5.

- [10] Lars Nielsen and Lars Eriksson. *Course Material Vehicular Systems*. Linköping Institute of Technology, 1998.
- [11] M. Nyberg. *Model Based Fault Diagnosis - Methods, Theory, and Automotive Engine Applications*. Linus & Linnea AB, 1999. ISBN 91-7219-521-5.
- [12] N. Watson and M.S. Janota. *Turbocharging the Internal Combustion Engine*. The Macmillan Press ltd, 1982. ISBN 0-333-24290-4.

Appendix A

Engine Simulation

Simulation of dynamic systems is mainly a question of solving systems of ordinary differential equations. This may seem easy, but is often quite tricky because of singularities and different magnitudes of time constants. These problems can cause unreasonable long simulation times and erroneous simulation results. A brief overview of different simulation topics is given in this chapter.

The first section deals with the crucial problem of solving the differential equations given by the model.

A.1 Solving Ordinary Differential Equations

In Simulink the engine model is represented as a block diagram with integrators as dynamic elements. To simulate the model it is necessary to transform the block diagram into a system of differential equations. A first order differential equation can be written as

$$\dot{x}(t) = f(x(t), u(t)) \quad (\text{A.1})$$

where $x(t)$ is the unknown variable. The order of the differential equation is equivalent to the highest derivative in the equation. Differential equations including derivatives with respect to more than one variable are referred to as *Partial Differential Equations* (PDE). Fortunately only first order *Ordinary Differential Equations* (ODE) are needed to describe the dynamics of the engine.

The following paragraphs show some different methods of solving these equations, starting with Euler's method which can be seen as a base for all the other methods presented.

A.1.1 Euler's Method

Evaluation of Equation (A.1) for the point $t = t_n$ yields

$$\dot{x}(t_n) = f(t_n, x(t_n)).$$

The derivative can now be replaced by the following discrete estimation

$$\dot{x}(t_n) \approx \frac{x(t_{n+1}) - x(t_n)}{h}.$$

The differential equation is thus transformed into a discrete difference equation

$$\frac{x(t_{n+1}) - x(t_n)}{h} \approx f(t_n, x(t_n)).$$

Replacement of $x(t_n)$ and $x(t_{n+1})$ with x_n and x_{n+1} respectively, result in a classical numerical method for solving differential equations. It is called *Euler's method*:

$$x_{n+1} = x_n + hf(t_n, x_n), \quad x_0 = \alpha \quad (\text{A.2})$$

α is a boundary condition at the starting point.

Equation (A.2) is a recursion formula and the results x_1, x_2, x_3, \dots are approximations to $x(t_1), x(t_2), x(t_3), \dots$. The errors that originate from the discretization process are called truncation errors. These errors depend of course on the step size h . Euler's method has a global truncation error which is $O(h)$, i.e. proportional to h .

Euler's method is simple but not particularly effective. It is however often used for simulations at crude tolerances. There are, as we soon will see, more effective methods.

A.1.2 Runge-Kutta Methods

Euler's method, which is a special case of the *Runge-Kutta methods*, uses the slope at the beginning of the interval as the representative slope over the interval. The more sophisticated Runge-Kutta methods do make better approximations of the slope over the interval. The version depicted here calculates the derivative approximations at four different points and a weighted average of the derivative in the interval. This value is then multiplied with the step length, h , and added to x_n to produce x_{n+1} . This method gives a global error of $O(h^4)$, which can be compared with the global error of $O(h)$ in Euler's method. One disadvantage is the fact that f has to be calculated four times.

Runge-Kutta's classical method:

$$\begin{aligned} k_1 &= hf(t_n, x_n) \\ k_2 &= hf(t_n + h/2, x_n + k_1/2) \\ k_3 &= hf(t_n + h/2, x_n + k_2/2) \\ k_4 &= hf(t_n + h, x_n + k_3) \end{aligned}$$

and

$$x_{n+1} = x_n + \frac{1}{6}(k_1 + 2k_2 + 2k_3 + k_4) \quad (\text{A.3})$$

Many solvers used in Simulink are based on Runge-Kutta methods, e.g. *ode45* and *ode23*. These solvers work best on non-stiff systems. Solvers for stiff systems are discussed in Section A.1.4.

A.1.3 A General Algorithm

A general method of how to solve differential equations can be written as

$$x_{n+1} = G(t, x_{n-k+1}, x_{n-k+2}, \dots, x_n, x_{n+1}) \quad (\text{A.4})$$

If G does not include x_{n+1} on the right hand side of Equation (A.4), we have an explicit method. This means that Euler's method, Equation (A.2), and the Runge-Kutta methods, Equation (A.3), are explicit. Methods that are not explicit are called implicit, and in that case we will have to solve an equation system to get a value of x_{n+1} .

The number k denotes the number of solutions from previous intervals that are used to predict the current value, x_{n+1} . Euler's method and the Runge-Kutta methods are obviously one step methods.

A.1.4 Stiff Differential Equations

Physical systems do often have both slow and fast dynamics. The engine described in this report is an example of this. The filling dynamics of the air filter, i.e. the smallest volume in the model, is fast in comparison with the turbine shaft dynamics and the filling dynamics of the larger volumes. The time constant of the air filter is about 100 times faster than the time constants of the other dynamic elements. The determination of time constants is done in Section 3.

According to [8] physical systems which have a ratio between the slowest and the fastest time constants, greater than 10-100 are considered as stiff. Hence, the system at hand here is stiff. Special methods are needed to solve stiff differential equations efficiently and the principles of such methods are discussed below.

To solve a stiff differential equation one must start with a short step size to follow the fast dynamics well. When the fast dynamics have reached stationary conditions, it is very ineffective to follow the slow dynamics with these very small steps. Consequently one wants to use a larger step size to follow the slow dynamics. This is when the difficulties arise. Stability problems may occur, if the step size in a numerical method is changed. There are however methods which can handle large step sizes as long as the differential equation itself is stable. Unfortunately, the large step sizes do cause bad simulation accuracy.

It should be noted that implicit methods often have better stability properties than explicit methods. This is the reason why implicit methods more often are used to solve stiff problems.

Simulink has several solvers for stiff differential equations, e.g. *ode15s* and *ode23s*.

A.1.5 Stability of Solutions

Stability is, as mentioned above, a very important property of the solutions. It is the stability properties of the differential equation in combination with the numerical method that are of interest in simulations. The following test equation can be used in order to investigate the stability properties of numerical methods

$$\begin{aligned}\dot{x} &= \lambda x, & \lambda \in \mathbf{C} \\ x(0) &= 1\end{aligned}$$

The equation is such that $x \rightarrow 0$ if $\operatorname{Re}\lambda < 0$ and $|x| \rightarrow \infty$ if $\operatorname{Re}\lambda > 0$. Obviously this equation has a very large stability region, which is one reason why it is a feasible test equation. Numerical methods which match it perfectly are rare and do not provide particularly accurate solutions. Such methods are, as mentioned above, primarily used for stiff problems where a variable step size is required. It is necessary to know the stability properties of the numerical method to be able to establish the stability of a dynamic system from simulations.

Euler's method is used here as an illustration of how to establish the convergence region of a numerical method. The ideas are applicable to more complex methods as well, but the calculations will then be more cumbersome. If Euler's method is applied to the test equation we will get

$$x_{n+1} = x_n + h\lambda x_n = (1 + h\lambda)x_n.$$

This equation can easily be solved by using the Z-transform. The result is

$$x_n = (1 + h\lambda)^n.$$

The difference equation will apparently converge if $|1 + h\lambda| < 1$. The convergence region is a circle which lies entirely within the convergence region of the test equation. The difference equation will therefore converge for sufficiently small step sizes, as long as the test equation is stable.

A.2 Literature

The main ideas in this chapter come from [8], [3] and [1].

Appendix B

User's Guide

A great deal of work has been done to make the model easy to use, but nevertheless a short information about the model might be helpful.

The engine has been divided in sub systems according to Figure B.1. Only the top level of the simulink model is shown here. It does not seem necessary to show the implementation of all the models of the subsystems as they have already been presented in Chapter 2.

In order to develop the simulation model further it facilitates to be able to change the parameter values in the model in a simple way. Therefore a Matlab m-file has been constructed where all model parameters are set and the values of these parameters can be changed if the engine is run under different ambient conditions or if new models are found for some part of the engine.

During the development of the simulation model it has turned out that it is crucial to choose the ODE-solver carefully. The simulations seem to be fastest and most accurate if ODE-solvers which are designed for stiff differential equations are used. Stiff differential equations were discussed in detail in Appendix A.

Initial values of the integrators should also be chosen with some precision. The initial values of the pressures were mostly chosen to agree with ambient conditions. When the engine does not run this assumption is physically correct. Consequently, it is of course desirable to start the turbocharger from rest as well, but doing so did unfortunately result in severe simulation difficulties. The simulations worked much better if the turbocharger was started at e.g. 80,000 RPM.

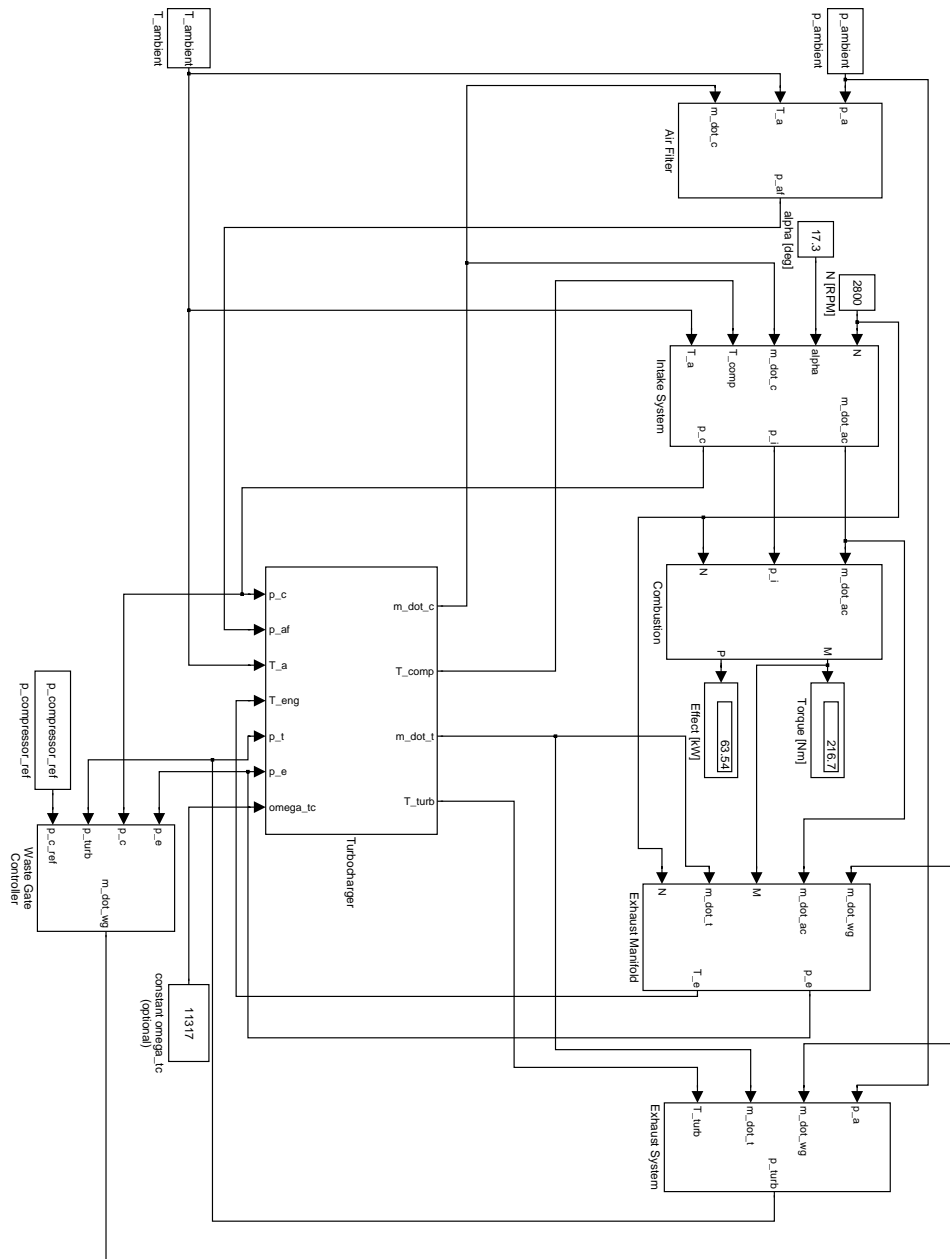


Figure B.1 The figure shows the top level of the Simulink model. N and α can easily be manipulated directly in Simulink, while many other parameters are possible to change via a Matlab m-function.